Prepared for submission to JHEP

Chiral dynamics in a magnetic field from the functional renormalization group

Kazuhiko Kamikado[a] **and Takuya Kanazawa**[b]

[a] *Theoretical Research Division, Nishina Center, RIKEN, Saitama 351-0198, Japan*
[b] *Quantum Hadron Physics Laboratory, RIKEN, Saitama 351-0198, Japan*

E-mail: kazuhiko.kamikado@riken.jp, takuya.kanazawa@riken.jp

Abstract: We investigate the quark-meson model in a magnetic field using the functional renormalization group equation beyond the local-potential approximation. Our truncation of the effective action involves anisotropic wave function renormalization for mesons, which allows us to investigate how the magnetic field distorts the propagation of neutral mesons. Solving the flow equation numerically, we find that the transverse velocity of mesons decreases with the magnetic field at all temperatures, which is most prominent at zero temperature. The meson screening masses and the pion decay constants are also computed. The constituent quark mass is found to increase with magnetic field at all temperatures, resulting in the crossover temperature that increases monotonically with the magnetic field. This tendency is consistent with most model calculations but not with the lattice simulation performed at the physical point. Our work suggests that the strong anisotropy of meson propagation may not be the fundamental origin of the inverse magnetic catalysis.

arXiv:1312.3124v2 [hep-ph] 13 Mar 2014

Contents

1 Introduction **1**

2 Functional renormalization group for the quark-meson model **3**
- 2.1 General structure of the flow and regulators 4
- 2.2 Scale-dependent effective action 4
- 2.3 Flow equations for the quark-meson model 6
- 2.4 Physical quantities 9

3 Numerical results **10**
- 3.1 Parameter fixing 11
- 3.2 Pseudo-critical temperature 12
- 3.3 Meson modes under magnetic field 14

4 Conclusion **18**

A Derivation of the flow equation for U_k **20**
- A.1 Bosonic contribution to $\partial_k U_k$ 20
- A.2 Fermionic contribution to $\partial_k U_k$ 21

B Derivation of the flow equations for $Z_k^\perp$ and $Z_k^\parallel$ **21**
- B.1 Bosonic contribution to $\partial_k Z_k$ 22
- B.2 Fermionic contribution to $\partial_k Z_k$ 26
  - B.2.1 Flow of $Z_k^\perp$ 28
  - B.2.2 Flow of $Z_k^\parallel$ 30

C Flow of the Taylor coefficients of U_k **31**

1 Introduction

Understanding strongly coupled dynamics of Quantum Chromodynamics (QCD) from first principles is one of the most important challenges in modern theoretical physics. Chiral symmetry breaking and quark confinement are two hallmarks of the nonperturbative QCD vacuum. Moreover QCD exhibits novel phenomena under extreme conditions, such as color deconfinement at high temperature and color superconductivity at high baryon chemical potential. These areas are actively investigated in relation to the physics of compact stars, heavy ion collisions, and early Universe; see [1] for a review.

Recently QCD in an external magnetic field has attracted considerable attention. The magnetic field is not only interesting as a theoretical probe to the dynamics of QCD, but also important in cosmology and astrophysics. A class of neutron stars called magnetars

has a strong surface magnetic field of order 10^{10} T [2] while the primordial magnetic field in early Universe is estimated to be even as large as $\sim 10^{19}$ T [3]. In non-central heavy ion collisions at RHIC and LHC, a magnetic field of strength $\sim 10^{15}$ T perpendicular to the reaction plane could be produced and can have impact on the thermodynamics of the quark-gluon plasma [4].

The effect of magnetic field has been vigorously investigated in chiral effective models [5–36] (see [37, 38] for reviews). It was found that the magnetic field acts as a catalyst of chiral symmetry breaking, an effect called *magnetic catalysis*. This model-independent phenomenon is explained through dimensional reduction ($3+1 \to 1+1$) in the quark pairing dynamics in a magnetic field [10, 11].

The dynamics of QCD in a magnetic field has also been studied in lattice simulations [39–52], see [53] for a review. At a relatively large quark mass, the chiral condensate and the chiral restoration temperature were found to increase with the magnetic field in accordance with the magnetic catalysis scenario,[1] whereas simulations at the physical quark masses [43, 46] show that the effect of a magnetic field is non-monotonic: the chiral condensate increases at low temperature, but *decreases* at high temperature, resulting in a lower pseudo-critical temperature in a stronger magnetic field. The origin of this *inverse magnetic catalysis* (or *magnetic inhibition*) is not fully understood yet.

Possible explanations for the inverse magnetic catalysis have been suggested by several groups [55–58]. Among others, Fukushima and Hidaka [55] noted that the dimensional reduction of neutral pion could be a source of disorder that weakens chiral symmetry breaking. The idea is rooted in the observation that the neutral pion 'feels' the magnetic field through its internal quark and anti-quark, and consequently the pion can move in directions transverse to the magnetic field with little energy cost [10, 11, 31, 32]. However the analysis of [55] was limited to zero temperature, and the impact of anisotropic fluctuations of neutral pion on the finite-temperature dynamics of QCD has not been quantitatively investigated.

In this work, we apply the functional renormalization group (FRG) [59] to the quark-meson model to study chiral symmetry breaking and its restoration at finite temperature under a magnetic field. FRG is a powerful nonperturbative method to go beyond the mean-field approximation by fully taking thermal and quantum fluctuations into account. The basic idea of FRG is to start from a microscopic action at the UV scale $k = \Lambda$, and keep track of the flow of the scale-dependent effective action while integrating out degrees of freedom with intermediate momenta successively; finally at $k = 0$ the full quantum effective action is obtained. See [60–63] for reviews. While FRG has already been applied to chiral models in a magnetic field [27–30, 35], so far no attempt has been made to go beyond the leading order of the derivative expansion, known as the *local-potential approximation* (LPA) in which the meson fluctuations are included but the scale-dependent flow of the kinetic term is entirely neglected. In this work, we proceed to the next order of the derivative expansion by including the wave function renormalization. This enables us to investigate the *strongly anisotropic* meson fluctuations for the first time. We will show that the pion

[1] However, *inverse* magnetic catalysis with large quark mass was reported quite recently [54].

decay constant and the meson screening masses become direction dependent, due to the breaking of the rotational symmetry by a magnetic field, and that the pion's *transverse velocity* (i.e. the velocity in the direction perpendicular to the magnetic field) decreases significantly under a strong magnetic field. [2] To be specific, we will compute following quantities as functions of temperature and magnetic field strength:

- Constituent quark mass (M_q)
- Transverse meson screening masses ($m^{\perp}_{\pi,\sigma}$)
- Longitudinal meson screening masses ($m^{\parallel}_{\pi,\sigma}$)
- Transverse pion decay constant ($f^{\perp}_{\pi}$)
- Longitudinal pion decay constant ($f^{\parallel}_{\pi}$)
- Wave function renormalization factors for mesons ($Z^{\perp}$, $Z^{\parallel}$)
- Transverse velocity of mesons ($v^2_{\perp} \equiv Z^{\perp}/Z^{\parallel}$)
- Chiral restoration temperature ($T_{\rm pc}$)

Our model calculations for the anisotropic screening masses and the transverse velocity of pions offer predictions that can be tested in future lattice simulations. As for the pseudo-critical temperature, contrary to the expectation from [55], we did not observe agreement with lattice data: $T_{\rm pc}$ *increases* monotonically with the magnetic field as in other model calculations, despite the fact that our present calculation incorporates significantly more meson fluctuations than other calculations. While our truncation of the effective action is still far from being complete and can be extended further, the discrepancy with lattice data could be taken as evidence that gluonic degrees of freedom which are ignored in chiral models actually play a vital role in the phenomenon of inverse magnetic catalysis.

This paper is organized as follows. In section 2 we introduce the quark-meson model and describe the formulation of FRG. We specify our truncation of the effective action and introduce regulators that are devised for analysis in a magnetic field. Then we give full expressions for the flow equations (omitting the details of derivation) and discuss the setup to solve them numerically. In section 3 we show plots of physical observables obtained with a numerical method, discuss their characteristics, and compare with the mean-field treatment and LPA. We will also comment on agreement and discrepancy with the available lattice data. Section 4 is devoted to conclusion. The analytical derivation of all the flow equations is presented in full details in appendices A, B, and C.

2 Functional renormalization group for the quark-meson model

In this section we describe the setup of FRG for the quark-meson model in a magnetic field. In general, FRG requires specification of the following 4 ingredients: (1) the flow equation, (2) regulator functions, (3) truncation of the effective action, and (4) initial conditions for the flow. We will describe (1)–(3) in this section and (4) in section 3.1.

[2] This is similar to the effect of the heatbath in finite-temperature QCD where the temporal decay constant differs from the spatial decay constant and the pion velocity is less than the speed of light [64–66].

2.1 General structure of the flow and regulators

The functional renormalization group equation (called the Wetterich equation) reads

$$\partial_k \Gamma_k = \frac{1}{2}\,\mathrm{Tr}\left[\frac{1}{\Gamma_k^{(2,0)} + R_k^B}\partial_k R_k^B\right] - \mathrm{Tr}\left[\frac{1}{\Gamma_k^{(0,2)} + R_k^F}\partial_k R_k^F\right], \tag{2.1}$$

which describes the evolution of the scale-dependent effective action Γ_k from the initial UV scale ($k = \Lambda$) to the IR limit ($k = 0$). $\Gamma_{k=\Lambda}$ is taken to be equal to the classical action and $\Gamma_{k=0}$ is the full quantum effective action incorporating the effects of all fluctuations. Here R_k^B and R_k^F are cutoff functions (regulators) for bosons and fermions, while $\Gamma_k^{(2,0)}$ and $\Gamma_k^{(0,2)}$ represent the second functional derivative of Γ_k with respect to boson fields and fermion fields, respectively. Tr is a trace in the functional space. Further details on FRG can be found in reviews [60–63].

Although (2.1) has a simple one-loop structure, it must be distinguished from the perturbative one-loop approximation: actually (2.1) incorporates effects of arbitrarily high order diagrams in the perturbative expansion through the full field-dependent propagator $(\Gamma_k^{(2)} + R_k)^{-1}$.

The flow of Γ_k from UV to IR is controlled by the cutoff functions $R_k^{B,F}(p)$. The latter must satisfy (i) $\lim_{k\to\infty} R_k(p) = \infty$, (ii) $\lim_{k\to 0} R_k(p) = 0$, and (iii) $\lim_{p\to 0} R_k(p) > 0$ [60]. In this work we use the following *anisotropic* regulators

$$R_k^B(p) = (k^2 - p_3^2) Z_k^{\parallel}\,\theta(k^2 - p_3^2)\,, \tag{2.2}$$

$$R_k^F(p) = -i\not{p}_3 r_k(p_3) \qquad \text{with} \qquad r_k(p_3) \equiv \left(\frac{k}{|p_3|} - 1\right)\theta(k^2 - p_3^2)\,, \tag{2.3}$$

for bosons and fermions ($\not{p}_3 = p_3\gamma_3$), respectively. Here $Z_k^{\parallel}$ is a wave function renormalization factor for mesons (cf. section 2.2). These regulators comply with the conditions (i)–(iii) above. Actually they are nothing but Litim's optimized regulator but now restricted to the p_3 direction. On one hand, these (somewhat unusual) regulators that break rotational symmetry are quite convenient because of a simple form of the scale-dependent fermion propagator in a magnetic field, as will be demonstrated later. On the other hand, they render the flow equation UV-divergent as they do not suppress momenta p_1 and p_2 at all. We will return to this problem later. Associated with this, we remark that the scale-dependent action Γ_k no longer admits a naive interpretation as a Wilsonian coarse-grained effective action at scale k, because the above regulators do not suppress modes with momenta $p_{1,2}^2 \lesssim k^2$. However, we hasten to add that those regulator functions work *perfectly well* as a machinery to interpolate between the classical action and the full quantum effective action.

2.2 Scale-dependent effective action

Next, let us define the model we use and specify our truncation of the running effective action. If we consider realistic QCD with two flavors of charge $+2e/3$ and $-e/3$, the chiral symmetry $\mathrm{SU}(2)_R \times \mathrm{SU}(2)_L \cong \mathrm{O}(4)$ would be *explicitly* broken even in the chiral limit and

consequently the flow equation becomes highly complicated: the scale-dependent effective potential would no longer be a function of the single $O(4)$-symmetric variable $\sigma^2+\vec{\pi}^2$, [3] and also the wave function renormalization factors for $\pi^\pm$ and π^0 will be different in general.

To avoid these complications and focus on the mechanism proposed by Fukushima and Hidaka [55], we will limit ourselves to the quark-meson model [67, 68] with *one flavor* of a fermion with charge e and color N_c. (We ignore the axial anomaly.) In this model, the pion (π) is neutral. Since $\pi^\pm$ in real $N_f = 2$ QCD decouple from the low-energy dynamics in a strong magnetic field and only the neutral pion π^0 remains light, it essentially reduces to the model considered here.

While the original Wetterich equation (2.1) formulated in the infinite-dimensional functional space is *exact*, in practice we need to find a proper truncation of Γ_k to make explicit computations feasible. A variety of truncation schemes have been discussed in the literature. Among others, the leading order of the derivative expansion, called the local-potential approximation (LPA), is frequently used due to its technical simplicity and was also employed in [27, 30, 35]. In LPA the effective potential flows with k while the field renormalization is neglected altogether, resulting in identically vanishing anomalous dimension of fields. In this work, we go beyond LPA by employing the following truncation of the running effective action:

$$\Gamma_k[\psi,\sigma,\pi] = \int_0^\beta dx_4 \int d^3x \left\{ \sum_{a=1}^{N_c} \overline{\psi}_a [\not{D} + g(\sigma + i\gamma_5 \pi)]\psi_a + U_k(\rho) - h\sigma \right. \\ \left. + \frac{Z_k^\perp}{2} \sum_{i=1,2} [(\partial_i \sigma)^2 + (\partial_i \pi)^2] + \frac{Z_k^\parallel}{2} \sum_{i=3,4} [(\partial_i \sigma)^2 + (\partial_i \pi)^2] \right\}, \tag{2.4}$$

with $\beta = 1/T$ and $\rho \equiv \frac{1}{2}(\sigma^2+\pi^2)$. The Dirac operator reads

$$\not{D} = \gamma_\mu D_\mu\,, \qquad D_\mu = \partial_\mu - ieA_\mu\,, \qquad \boldsymbol{A} = (0, Bx_1, 0)\,, \quad \text{and} \quad A_4 = 0\,. \tag{2.5}$$

One can verify that the action possesses $\mathrm{U}(1) \times \mathrm{U}(1)$ chiral symmetry when $h = 0$. The parameter h that enters as a symmetry breaking field parametrizes the effect of current quark mass. Below we assume $h > 0$. In (2.4) we introduced the wave function renormalization factors $Z_k^\perp$ and $Z_k^\parallel$. Setting $Z_k^\perp = Z_k^\parallel = 1$ brings us back to LPA. Here we let these variables depend on k. It is important that $Z_k^\perp$ for directions perpendicular to the magnetic field, and $Z_k^\parallel$ for directions parallel to the magnetic field, are treated independently. This setup is well-motivated in view of the anisotropy induced by a magnetic field and is actually essential to test the scenario by Fukushima and Hidaka [55].

Several caveats are in order. Firstly, we neglect the wave function renormalization of fermions and the derivative term of ρ (i.e., $(\partial_\mu \rho)^2$), as well as all bosonic terms that are consistent with symmetries and include more than two derivatives. We also ignore the k-dependence of g because the flow of g is not expected to affect final results significantly (see e.g., [67]). In principle all these corrections can be incorporated into the present approach in

[3] This point seems to have been neglected in earlier works [27, 30, 35].

a straightforward manner,[4] but it is beyond the scope of this work. Secondly, for technical simplicity, we use a common variable, $Z_k^{\parallel}$, for both the wave function renormalization factor in x_4-direction and that in x_3-direction. We assume the error due to this approximation is small (see [71] for a discussion on a related issue at finite temperature).

2.3 Flow equations for the quark-meson model

With (2.1), (2.2), (2.3) and (2.4), we are now ready to derive the flow equations for $U_k(\rho)$, $Z_k^{\perp}$ and $Z_k^{\parallel}$ explicitly. Since their analytical derivation is rather lengthy and involved, we shall relegate it to the appendices A and B. Here we only quote the main formulas:

$$\partial_k U_k(\rho) = k^2 \left(1 + \frac{k}{3}\frac{\partial_k Z_k^{\parallel}}{Z_k^{\parallel}}\right) \int' \frac{d^2p_\perp}{(2\pi)^3} \left(\frac{1}{E_\pi(\rho)} \coth\frac{E_\pi(\rho)}{2T} + \frac{1}{E_\sigma(\rho)} \coth\frac{E_\sigma(\rho)}{2T}\right) - \frac{1}{2\pi^2} N_c k^2 |eB| \sum_{n=0}^{\infty}{}' \frac{\alpha_n}{E_n(\rho)} \tanh\frac{E_n(\rho)}{2T}\,, \tag{2.6}$$

$$\partial_k Z_k^{\perp} = -\frac{k^2}{\pi^2} \frac{\overline{\rho}_k \left[U_k''(\overline{\rho}_k)\right]^2}{(Z_k^{\parallel})^2} \left(1 + \frac{k}{3}\frac{\partial_k Z_k^{\parallel}}{Z_k^{\parallel}}\right) T \sum_{q_4:\,\text{even}} \int_0^\infty \frac{dw}{\left(w + k^2 + q_4^2 + \frac{\hat{m}_\pi^2}{Z_k^{\parallel}}\right)^2 \left(w + k^2 + q_4^2 + \frac{\hat{m}_\sigma^2}{Z_k^{\parallel}}\right)^2} - \frac{1}{\pi^2} N_c g^2 k^2\, T \sum_{q_4:\,\text{odd}} \frac{1}{[q_4^2 + E_0(\overline{\rho}_k)^2]^2}\,, \tag{2.7}$$

$$\partial_k Z_k^{\parallel} = -\frac{k^2}{\pi^2} \frac{\overline{\rho}_k \left[U_k''(\overline{\rho}_k)\right]^2}{Z_k^{\parallel} Z_k^{\perp}} T \sum_{q_4:\,\text{even}} \int_0^\infty \frac{dw}{\left(w + k^2 + q_4^2 + \frac{\hat{m}_\pi^2}{Z_k^{\parallel}}\right)^2 \left(w + k^2 + q_4^2 + \frac{\hat{m}_\sigma^2}{Z_k^{\parallel}}\right)^2} - \frac{1}{2\pi^2} N_c g^2 |eB|\, T \sum_{q_4:\,\text{odd}} \sum_{n=0}^{\infty} \frac{\alpha_n}{[q_4^2 + E_n(\overline{\rho}_k)^2]^2}\,, \tag{2.8}$$

with the definitions

$$U_k' \equiv \partial U_k/\partial\rho\,, \qquad U_k'' \equiv \partial^2 U_k/\partial\rho^2\,, \tag{2.9}$$

$$\alpha_n \equiv \begin{cases} 1 & (n=0) \\ 2 & (n \geq 1) \end{cases}\,, \qquad E_n(\rho) \equiv \sqrt{k^2 + 2|eB|n + 2g^2\rho}\,, \tag{2.10}$$

$$E_\pi(\rho) \equiv \sqrt{k^2 + \frac{Z_k^{\perp} p_\perp^2 + U_k'(\rho)}{Z_k^{\parallel}}}\,, \quad E_\sigma(\rho) \equiv \sqrt{k^2 + \frac{Z_k^{\perp} p_\perp^2 + U_k'(\rho) + 2\rho U_k''(\rho)}{Z_k^{\parallel}}}\,, \tag{2.11}$$

$$\overline{\rho}_k \equiv \underset{\rho>0}{\text{argmin}} \left\{U_k(\rho) - h\sqrt{2\rho}\right\}, \tag{2.12}$$

$$\hat{m}_\pi^2 \equiv U_k'(\overline{\rho}_k)\,, \qquad \hat{m}_\sigma^2 \equiv U_k'(\overline{\rho}_k) + 2\overline{\rho}_k U_k''(\overline{\rho}_k)\,, \tag{2.13}$$

$$\sum_{q_4:\,\text{odd}} \equiv \sum_{\substack{\ell=-\infty \\ q_4=(2\ell+1)\pi T}}^{\infty}\,, \qquad \sum_{q_4:\,\text{even}} \equiv \sum_{\substack{\ell=-\infty \\ q_4=2\ell\pi T}}^{\infty}\,. \tag{2.14}$$

[4] See however [69, 70] for a subtlety in the higher-order derivative expansion based on a non-smooth regulator, such as Litim's optimized regulator. This issue does not arise at the order of expansion considered in this paper.

The meson masses (2.13) are *bare masses*, which should not be confused with the renormalized (physical) masses introduced later in section 2.4. The two primes ($'$) in (2.6) imply that the sum and the integral are divergent; we will comment more on this below. As one can see from the presence of $\partial_k Z_k^{\parallel}$ in the RHS of (2.6) and (2.7), the flow of U_k and $Z_k^{\perp}$ depend on the flow of $Z_k^{\parallel}$, whereas the flow of $Z_k^{\perp}$ and $Z_k^{\parallel}$ depend on U_k through $\overline{\rho}_k$. Thus these three coupled equations must be solved simultaneously. We note that (2.6) does not agree with the flow equations in [27, 30, 35] even for $Z_k^{\perp} = Z_k^{\parallel} = 1$, because the regulator we use is entirely different from those in [27, 30, 35]. The formulas (2.6), (2.7) and (2.8) can be simplified analytically so as to facilitate numerical evaluation; see the appendices A and B for details.

Even without relying on numerical analysis, one can understand to some extent the dynamics of the system through inspection of these flow equations. The second term in $\partial_k U_k(\rho)$, (2.6), originates from the fermionic contribution to the flow equation (cf. (2.1)). The summation over n manifestly embodies the Landau level structure of fermion's energy levels, and the lowest ($n = 0$) Landau level becomes dominant in a strong magnetic field. The fact that the prefactor which is normally k^4 [72–74] is now replaced by $k^2|eB|$ in (2.6) implies that the dynamics of fermions in a strong magnetic field is effectively reduced to $(1+1)$-dimensions. This illustrates how the *dimensional reduction* [10, 11] in the fermionic sector takes place.

What is more nontrivial is the dimensional reduction *in the bosonic sector* [55]. In our FRG setup, the only source of anisotropy of meson dynamics is the asymmetry between $\partial_k Z_k^{\perp}$ and $\partial_k Z_k^{\parallel}$. An important difference between them is that $\partial_k Z_k^{\perp}$ has no explicit dependence on eB in contrast to $\partial_k Z_k^{\parallel}$; one can anticipate that this feature will make $Z_k^{\perp}$ less sensitive to eB than $Z_k^{\parallel}$, which turns out to be true as demonstrated in section 3. Another notable difference is that the fermionic contribution in (2.7) is multiplied by k^2 whereas that in $\partial_k Z_k^{\parallel}$ is multiplied by $|eB|$. This means that the growth of $Z_k^{\parallel}$ toward $k = 0$ should be enhanced in a strong magnetic field, while no such effect is present for $Z_k^{\perp}$. These two characteristics of $\partial_k Z_k^{\perp}$ and $\partial_k Z_k^{\parallel}$ provide a rough understanding on how and why the magnetic field induces anisotropy in the propagation of neutral mesons.

Taylor expansion method In order to make the flow equation numerically more tractable, we expand the effective potential as a polynomial around the minimum:

$$U_k(\rho) = \sum_{n=0}^{2} a_k^{(n)} \frac{(\rho - \overline{\rho}_k)^n}{n!}\,, \tag{2.15}$$

$$\overline{\rho}_k \equiv \operatorname*{argmin}_{\rho} \left\{ U_k(\rho) - h\sqrt{2\rho} \right\}. \tag{2.16}$$

Note that $a_k^{(1)}$ is nonzero since $\overline{\rho}_k$ is not a minimum of $U_k(\rho)$. The expansion up to second order in ρ is normally sufficient to describe a second-order phase transition [75]. Then the

flows of $a_k^{(1)}$ and $a_k^{(2)}$ are easily found as

$$\partial_k a_k^{(1)} = \frac{\partial_k U_k'\big|_{\overline{\rho}_k}}{1 + \dfrac{(2\overline{\rho}_k)^{3/2}}{h} a_k^{(2)}} \qquad \text{and} \qquad \partial_k a_k^{(2)} = \partial_k U_k''\big|_{\overline{\rho}_k}\,, \tag{2.17}$$

while $\overline{\rho}_k$ is determined from the relation $\overline{\rho}_k = \dfrac{h^2}{2\big(a_k^{(1)}\big)^2}$ at each step of the flow. (The flow of $a_k^{(0)}$ is simply ignored as it plays no dynamical role.) One can derive $\partial_k U_k'$ and $\partial_k U_k''$ from (2.6) by taking derivatives with respect to ρ (see the appendix C for final expressions). The flow equations for $Z_k^{\perp}$ and $Z_k^{\parallel}$ are readily obtained from (2.7) and (2.8) upon substitution of (2.15). Now the problem reduces to solving coupled ordinary differential equations for five variables: $\overline{\rho}_k$, $a_k^{(1)}$, $a_k^{(2)}$, $Z_k^{\perp}$ and $Z_k^{\parallel}$.

Problem of UV renormalization It is intriguing to observe that the UV divergence encountered in (2.6) *disappears* once we take the derivative of $\partial_k U_k$ with ρ: both the integral and the sum are convergent. This means that the UV divergence only appears in the constant term of $U_k(\rho)$. Therefore, within the Taylor expansion scheme described above, *no* UV cutoff is necessary to make the flows of $a_k^{(1)}$ and $a_k^{(2)}$ finite! The full expressions of $\partial_k U_k'\big|_{\overline{\rho}_k}$ and $\partial_k U_k''\big|_{\overline{\rho}_k}$ obtained without UV cutoff are lengthy and are presented in the appendix C.

In principle one could also argue that an explicit UV cutoff has to be applied because the quark-meson model is after all a *low-energy* effective model of QCD. To assess the sensitivity of infrared observables to the UV regularization scheme, we have also solved the flow equations *with* an explicit UV cutoff ~ 1 GeV and compared the obtained results with those from the cutoff-free scheme. We found that while quantitative differences are present, the global tendencies of results from both schemes are the same, including the monotonic increase of $T_{\rm pc}$ as a function of eB. Therefore we will only present the numerical results obtained within the *cutoff-free* scheme in the next section.

LPA and mean-field approximation Finally, let us comment on other related schemes. In LPA we ignore nontrivial scale dependence of the propagators, which amounts to setting $Z_k^{\perp} = Z_k^{\parallel} \equiv 1$ in (2.6). This approximation has been employed to study chiral models in a magnetic field [27, 30, 35].

The conventional mean-field approximation is attained from our flow equation by setting bosonic fields to their expectation values and removing the bosonic loop contribution in (2.6) altogether. The resulting flow equation now reads

$$\partial_k U_k(\rho) = -\frac{1}{2\pi^2} N_c k^2 |eB| \sum_{n=0}^{\infty}{}' \frac{\alpha_n}{E_n(\rho)} \tanh\frac{E_n(\rho)}{2T}\,. \tag{2.18}$$

It is instructive to integrate both sides over k explicitly:

$$U_{k=0}(\rho) = U_{k=\Lambda}(\rho) - \int_0^\Lambda dk \left[-\frac{1}{2\pi^2} N_c k^2 |eB| {\sum_{n=0}^{\infty}}' \frac{\alpha_n}{E_n(\rho)} \tanh \frac{E_n(\rho)}{2T} \right] \tag{2.19}$$

$$= U_{k=\Lambda}(\rho) + 4N_c T \frac{|eB|}{2\pi} {\sum_{n=0}^{\infty}}' \alpha_n \int_0^\Lambda \frac{dk}{2\pi}\, k \frac{\partial}{\partial k} \left(\log\cosh \frac{E_n(\rho)}{2T} \right) \tag{2.20}$$

$$= U_{k=\Lambda}(\rho) - N_c \frac{|eB|}{2\pi} {\sum_{n=0}^{\infty}}' \alpha_n \int_{-\Lambda}^\Lambda \frac{dp_3}{2\pi} \left[E_n(\rho) + 2T \log(1 + \mathrm{e}^{-E_n(\rho)/T}) \right], \tag{2.21}$$

where in the last step we have discarded an irrelevant constant and a surface term resulting from partial integration, and relabelled k as p_3 so that $E_n(\rho) = \sqrt{p_3^2 + 2|eB|n + 2g^2\rho}$ can be interpreted as the energy of a quark in the n-th Landau level. As claimed above, (2.21) reproduces the thermodynamic potential in the mean-field approximation [19, 21]. The expectation value of ρ should be determined from the minimization of $U_{k=0}(\rho) - h\sqrt{2\rho}$.

2.4 Physical quantities

Let us define physical quantities attained in the $k \to 0$ limit of the flow equation. The essence is that the minimum of the effective potential gives the condensate $\langle\sigma\rangle$ while the curvature around the minimum gives the meson masses. In the presence of the field renormalization, however, these quantities are nontrivially renormalized and care must be taken in comparing results from FRG with those from other methods, such as lattice simulations. In this subsection we wish to spell out the notations and definitions of all observables we consider, as a preparation for section 3 where they are evaluated by numerically solving the flow equation.

Firstly, the dynamical quark mass is given by

$$M_q \equiv g f_\pi^{\mathrm{bare}} = g\sqrt{2\overline{\rho}_{k=0}}\,, \tag{2.22}$$

where $f_\pi^{\mathrm{bare}} = \langle\sigma\rangle$ is the *bare* pion decay constant. ($\langle\sigma\rangle > 0$ for $h > 0$.)

Next, we note that the dispersion of the mesons follows from (2.4) via analytic continuation as

$$Z_k^{\parallel} p_0^2 - Z_k^{\perp}(p_1^2 + p_2^2) - Z_k^{\parallel} p_3^2 - \hat{m}_{\sigma,\pi}^2 = 0\,, \tag{2.23}$$

with the *bare* masses $\hat{m}_{\sigma,\pi}$ defined in (2.13). Thus the screening mass in the directions orthogonal to the magnetic field (i.e., the *transverse* screening mass), $m_{\sigma,\pi}^{\perp}$, and the screening mass along the direction of the magnetic field (i.e., the *longitudinal* screening mass), $m_{\sigma,\pi}^{\parallel}$, are given by

$$m_{\sigma,\pi}^{\perp} \equiv \frac{\hat{m}_{\sigma,\pi}}{\sqrt{Z_{k=0}^{\perp}}} \qquad \text{and} \qquad m_{\sigma,\pi}^{\parallel} \equiv \frac{\hat{m}_{\sigma,\pi}}{\sqrt{Z_{k=0}^{\parallel}}}\,, \tag{2.24}$$

respectively. The *pole mass* is equal to $m_{\sigma,\pi}^{\parallel}$ within our effective action. It is also evident from (2.23) that the transverse velocity $v_\perp$ of mesons (i.e., the velocity of mesons in the

directions perpendicular to the magnetic field) is given by [5]

$$v_\perp \equiv \sqrt{\frac{Z^\perp_{k=0}}{Z^\parallel_{k=0}}}\,. \tag{2.25}$$

It has been suggested in model calculations that $v_\perp^2 \ll 1$ in a strong magnetic field [10, 11, 31, 32, 55] and it is one of our aims to check this at finite temperature in the framework of FRG, incorporating the effect of fluctuations of interacting mesons.

Interestingly, in the presence of a magnetic field the decay constant of the neutral pion also exhibits anisotropy [32]. This is due to the fact that the coupling of pions to the axial vector current is direction-dependent in a magnetic field. Although the definition of a 'decay constant' in a thermal media is nontrivial (see e.g., [64–66]), following [67, 68] we shall define the *transverse* and *longitudinal* pion decay constants at finite temperature by

$$f_\pi^\perp \equiv \sqrt{Z^\perp_{k=0}}\, f_\pi^{\rm bare} = \sqrt{2Z^\perp_{k=0}\bar{\rho}_{k=0}} \quad \text{and} \tag{2.26}$$

$$f_\pi^\parallel \equiv \sqrt{Z^\parallel_{k=0}}\, f_\pi^{\rm bare} = \sqrt{2Z^\parallel_{k=0}\bar{\rho}_{k=0}}\,, \tag{2.27}$$

respectively. This convention is motivated by the fact that the chiral effective Lagrangian of the neutral pion to lowest order assumes a particularly simple form

$$\mathcal{L}_{\rm eff} = \frac{f_\pi^{\perp 2}}{4}(\partial_\perp U)^2 + \frac{f_\pi^{\parallel 2}}{4}(\partial_\parallel U)^2 + \dots\,, \tag{2.28}$$

where $U(x)$ is a U(1) field whose phase describes the pion, $\partial_\perp = (\partial_1, \partial_2)$ and $\partial_\parallel = (\partial_3, \partial_4)$. In the limit of a weak magnetic field, $f_\pi^\perp / f_\pi^\parallel \to 1$ and $\mathcal{L}_{\rm eff}$ reduces to the familiar form.

This completes the formulation of FRG for the quark-meson model.

3 Numerical results

In this section we will show results of integrating the flow equations numerically. In order to estimate the impact of mesonic fluctuations, we will contrast results from three approximations: LPA plus scale-dependent wave function renormalizations (which we term "full FRG"), LPA, and the mean-field approximation.

One of our purposes is to understand the phase structure from the viewpoint of chiral symmetry. After describing the initial conditions of the flow in section 3.1, we will present results for the constituent quark mass (M_q) at finite temperature and magnetic field in section 3.2. From the temperature dependence of M_q the pseudo-critical temperature of the chiral phase transition is estimated and its dependence on the magnetic field is examined.

The neutral meson dynamics acquires anisotropy in an external magnetic field through the quark loop contributions. The second purpose of our FRG analysis is to see the anisotropy of neutral meson modes. In section 3.3, we calculate some observables such as meson screening masses, and examine their directional dependence at finite temperature and external magnetic field.

[5] Strictly speaking, $v_\perp$ in (2.25) is equal to the transverse velocity of mesons only when $m_{\sigma,\pi} = 0$. However we stick to calling this quantity the velocity for brevity.

	N_c	g	Λ	h/Λ^3	$a^{(1)}_{k=\Lambda}/\Lambda^2$	$a^{(2)}_{k=\Lambda}$	$Z^{\parallel}_{k=\Lambda}$	$Z^{\perp}_{k=\Lambda}$
Full FRG	3	2.0	600	0.00596	0.489	1.0	0.002	0.236
LPA	3	2.76	600	0.00835	0.732	5.0	—	—
Mean field	3	2.76	600	0.00820	0.947	0.25	—	—

Table 1. Initial conditions for the flow equation at $k = \Lambda$. The column for Λ is given in MeV.

	Observables at $k = 0$					$T_{\rm pc}$
	f_π	m_π	m_σ	M_q	$Z^{\parallel,\perp}_{k=0}$	
Full FRG	93.4*	138*	411*	257	0.529	178
LPA	94.2	138	407	260	—	194
Mean field	92.5	138	417	261	—	174

Table 2. Resulting physical values at $T = 3$ MeV and $eB = 0.5m_\pi^2$ and the pseudo-critical temperature $T_{\rm pc}$ at $eB = 0.5m_\pi^2$. The columns for f_π, m_π, m_σ, M_q and $T_{\rm pc}$ are given in MeV. The values with star * (f_π, m_π and m_σ for Full FRG) are obtained after the wave function renormalization (see section 2.4).

3.1 Parameter fixing

We numerically solved the Taylor-expanded flow (2.17) with the second-order Runge-Kutta method (RK2) for full FRG, LPA, and the mean-field approximation, respectively. The initial scale of the RG flow is fixed at 600 MeV. In LPA and the mean-field approximation, we have four initial parameters: $a^{(1)}_{k=\Lambda}$, $a^{(2)}_{k=\Lambda}$, h and g. In the full FRG calculation, in addition, we need to specify initial values for the wave function renormalizations, $Z^{\perp}$ and $Z^{\parallel}$. All those initial conditions are gathered in Table 1.

In Table 2, resulting physical values at $k = 0$ are shown for each approximation at $T = 3$ MeV and $eB = 0.5m_\pi^2$. (We checked that observables hardly vary for $0 \lesssim eB \lesssim 0.5m_\pi^2$, so $eB = 0.5m_\pi^2$ is small enough to be considered as the limit of vanishing magnetic field.) The initial flow parameters were tuned in each approximation so as to reproduce physical values for M_q, m_π, m_σ and f_π. This makes our model a good laboratory for QCD in the real world. As explained in section 2.4, the values of physical observables in the full FRG calculation (m_π, m_σ and f_π) are subject to the wave function renormalization.

In vacuum ($T = eB = 0$), the Euclidean SO(4) symmetry is intact. However this is not automatically realized in our setup due to the fact that the regulators used here ((2.2) and (2.3)) break the SO(4) symmetry *explicitly*, regardless of the magnetic field strength and temperature. Indeed $\partial_k Z^{\perp}_k$ in (2.7) does not agree with $\partial_k Z^{\parallel}_k$ in (2.8) even in the vacuum limit (T, $eB \to 0$). We cure this problem by fine-tuning the initial conditions $Z^{\perp,\parallel}_{k=\Lambda}$ so that $Z^{\perp}_{k=0} = Z^{\parallel}_{k=0}$ holds at $T = 3$ MeV and $eB = 0.5m_\pi^2$. This is how $Z^{\perp,\parallel}_{k=\Lambda}$ in Table 1 are fixed. We have used the same set of initial values at all temperatures.[6]

In Table 2, we also summarize the pseudo-critical temperature ($T_{\rm pc}$) in each approxi-

[6]The deviation of $Z^{\perp}_{k=0}/Z^{\parallel}_{k=0}$ from 1 turns out to be at most 10% over the range $0 < T < 360$ MeV at $eB = 0.5m_\pi^2$.

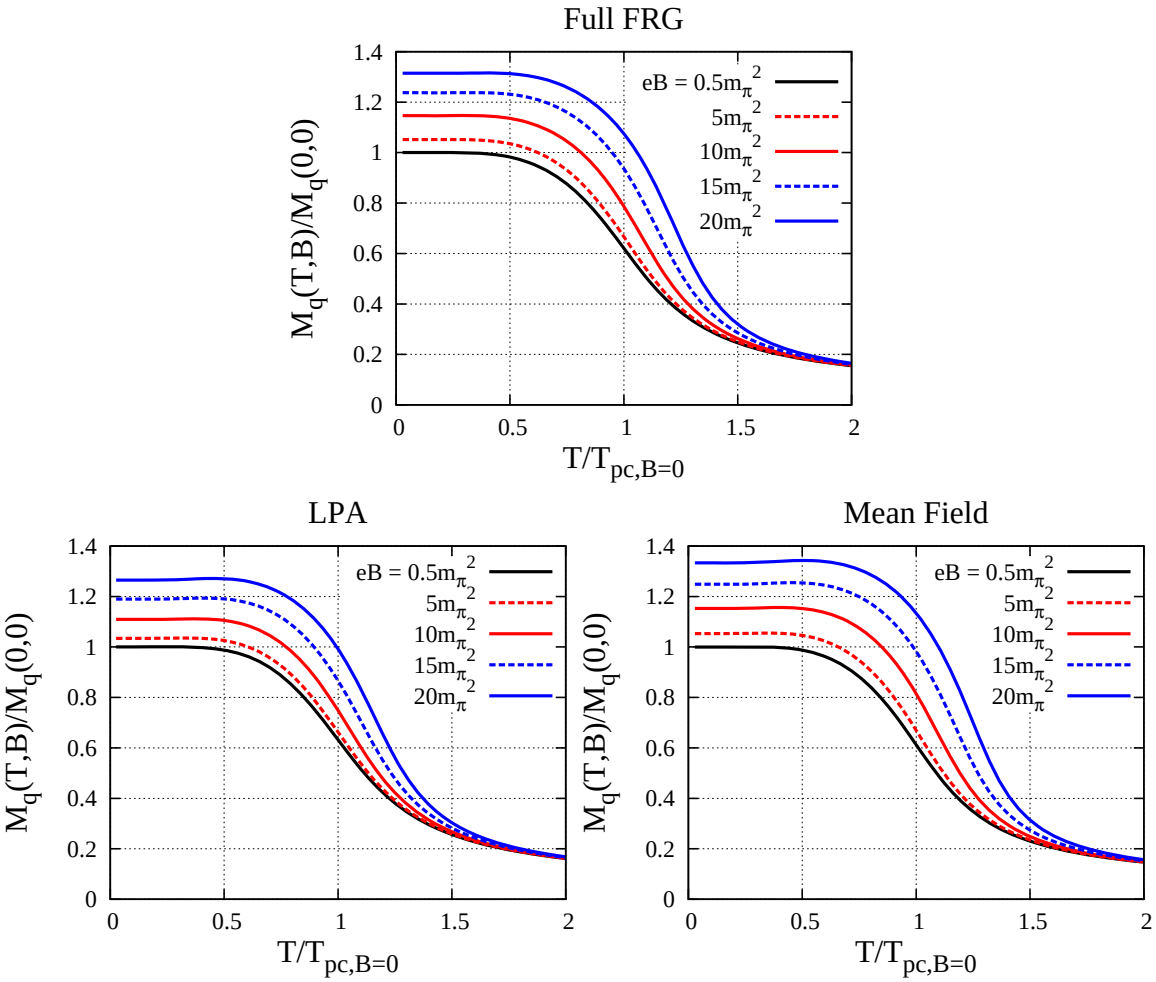


Figure 1. The constituent quark mass at finite temperature and magnetic field from full FRG (top), LPA (bottom, left) and the mean-field approximation (bottom, right). The vertical axis is normalized to 1 at $T = eB = 0$.

mation scheme at $eB = 0.5m_\pi^2$. Here $T_{\rm pc}$ is determined from the peak of the temperature derivative of the constituent quark mass. In the following subsections, we shall normalize the temperature axis of every plot by $T_{\rm pc}$ at $eB = 0.5m_\pi^2$ to facilitate comparison of the three approximations.

3.2 Pseudo-critical temperature

The constituent quark mass M_q is proportional to the bare pion decay constant (cf. (2.22)) and serves as an order parameter for the chiral symmetry breaking. In Fig. 1, we show the temperature dependence of M_q in full FRG, LPA, and the mean-field approximation, with varying external magnetic field. The three plots share the same qualitative features. At low temperature, chiral symmetry is spontaneously broken and quarks acquire a mass of order 300 MeV. At high temperature, chiral symmetry is effectively restored: the dynamical mass drops to around 15% of the vacuum value at $T = 2T_{\rm pc}$. Since quarks have the current mass, M_q never reaches zero even above $T_{\rm pc}$.

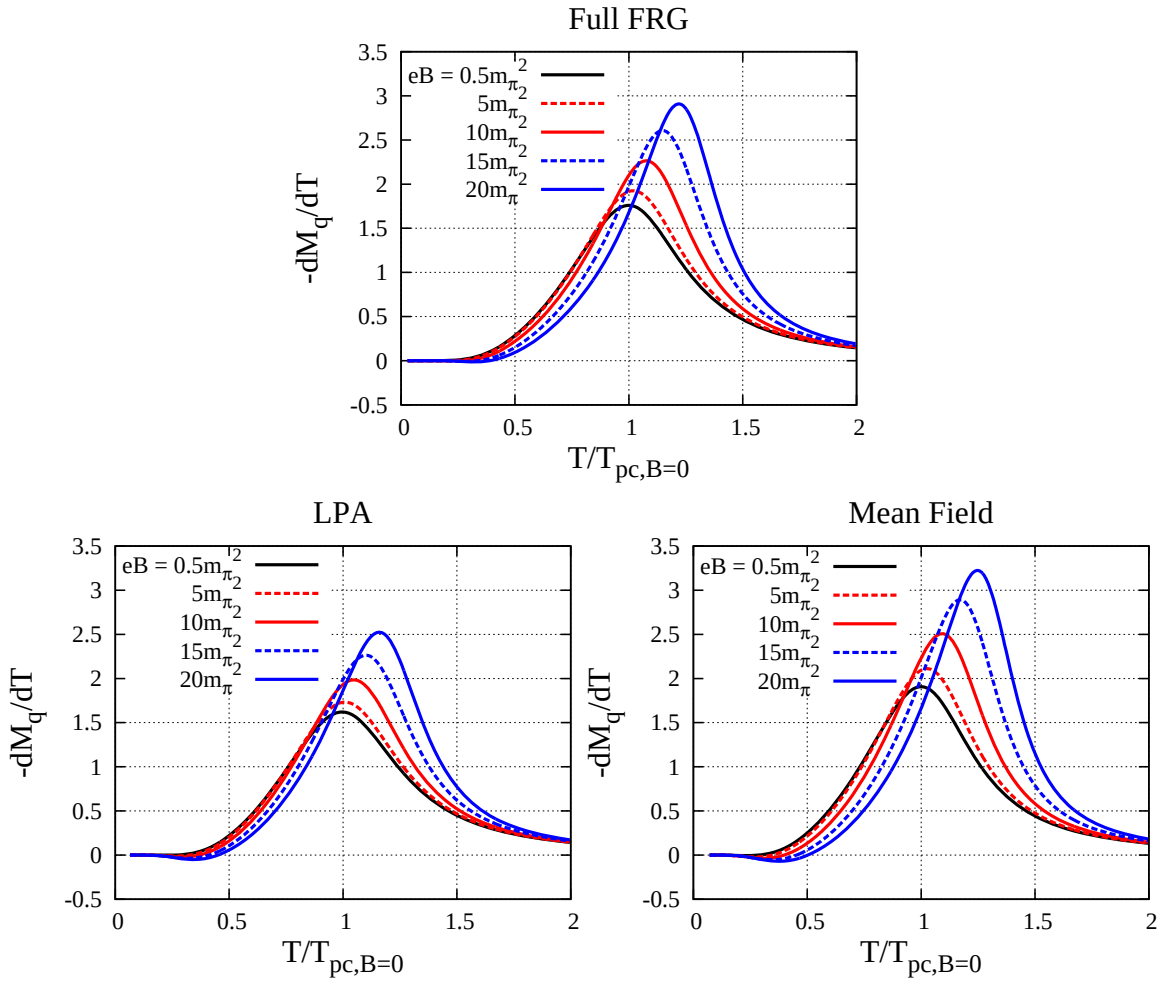


Figure 2. The slope of the constituent quark mass at finite temperature and magnetic field from full FRG (top), LPA (bottom, left) and the mean-field approximation (bottom, right).

From Fig. 1 one can read off the external magnetic field dependence of the constituent quark mass. In all the three approximations, M_q increases monotonically with $|eB|$ at all temperatures below $2T_{\rm pc}$. This behavior, called magnetic catalysis, has been observed in lattice simulations [53] as well as in various chiral effective models [38]. The increase of M_q with $|eB|$ is slower in LPA than in the mean-field approximation, which is attributable to the meson-loop contribution to the flow of U_k that counteracts the symmetry breaking effect of fermions. On the other hand, our new result from full FRG, which also includes effects of the wave function renormalization, turns out to be closer to the mean-field approximation than LPA.

In Fig. 2 we show the temperature derivative of M_q for various values of the external magnetic field. The peaks of these curves define the pseudo-critical temperature, $T_{\rm pc}$. Clearly, in all approximations, the peak temperature moves to a higher value for a stronger magnetic field. This tendency is consistent with many other works based on chiral effective models. However this is at odds with the recent lattice QCD calculation with light quarks

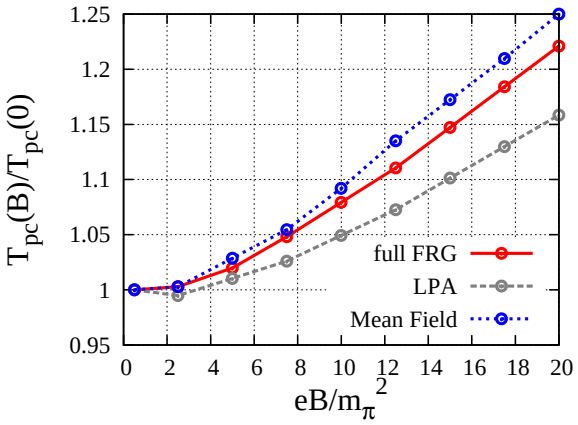


Figure 3. Magnetic field dependence of the pseudo-critical temperatures from three approximations.

[43, 46]. The plots in Fig. 2 suggest that the inclusion of the wave function renormalization alone does not resolve the discrepancy between the lattice QCD and chiral effective models.

In Fig. 3, we plot the pseudo-critical temperature versus magnetic field (in units of m_π^2) for each approximation. In all the three cases $T_{\rm pc}$ rises monotonically with $|eB|$, and $T_{\rm pc}$ in LPA and full FRG shows a milder increase than $T_{\rm pc}$ in the mean-field approximation, owing to the effect of mesonic fluctuations. This tendency is in discord with the previous work with two light flavors [27], where $T_{\rm pc}$ of LPA showed a stronger increase than that of the mean field. We speculate that the difference comes from the absence of the charged pions in our work.

Figure 3, somewhat unexpectedly, also shows that $T_{\rm pc}$ from full FRG rises *more steeply than* $T_{\rm pc}$ of LPA and behaves like that of the mean-field approximation. In the next subsection we will try to give a possible explanation to this trend based on the pion pole mass behavior at finite temperature.

3.3 Meson modes under magnetic field

In the last subsection we discussed the dynamical quark mass and the chiral restoration temperature. In what follows, we will present and discuss results related to the meson properties. The neutral mesons change their nature under strong external magnetic field because they are made of charged quarks. The most prominent feature is an anisotropy of the neutral meson modes. To investigate this issue in a quantitative manner we have calculated various observables related to the anisotropy of the neutral meson modes.

Let us begin with the wave function renormalization factors, which are the most central objects in our beyond-LPA analysis. In Fig. 4 we show $Z^{\parallel}$ and $Z^{\perp}$ at finite temperature and external magnetic field. There one can observe several marked features:

- **(a)** At high temperature, both $Z^{\parallel}$ and $Z^{\perp}$ diminish substantially and become insensitive to the magnetic field.
- **(b)** $Z^{\parallel}$ *increases* sharply with $|eB|$.
- **(c)** By contrast, $Z^{\perp}$ *decreases* with $|eB|$. However $Z^{\perp}$ shows only weak dependence on $|eB|$ at all temperatures.

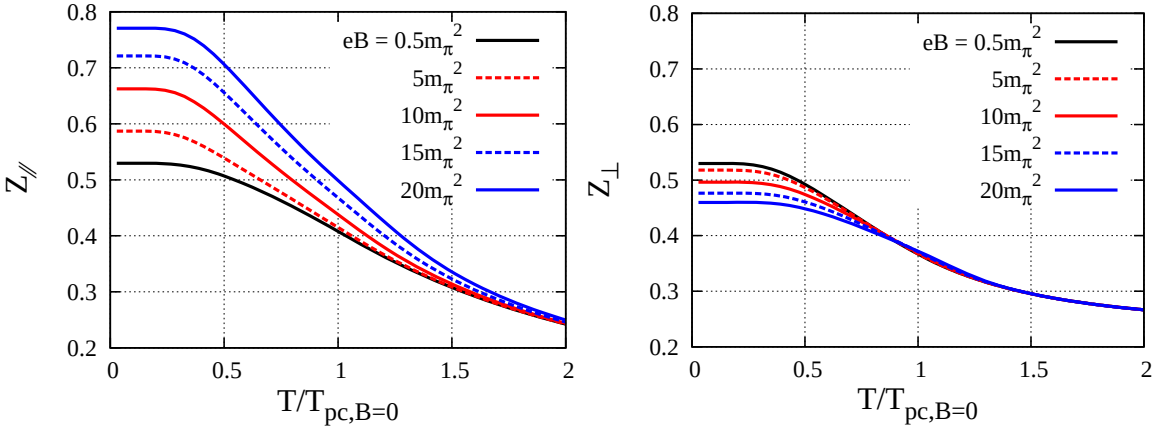


Figure 4. Parallel (left) and perpendicular (right) wave function renormalization factors of mesons.

These features can be understood, at least qualitatively, from the flow equations in (2.7) and (2.8). First of all, we remark that the meson contributions to $\partial_k Z_k^{\parallel}$ and $\partial_k Z_k^{\perp}$ are suppressed at all temperatures, except for the vicinity of $T_{\rm pc}$. (We have checked this explicitly by numerically integrating the flow equation.) The reason is as follows. In the meson loop diagram (cf. Fig. 10), both σ and π are circulating around the loop. Since σ is always heavy (except near $T_{\rm pc}$) and π also gets heavy at high temperature, the meson loop contribution turns out to be always suppressed as compared to the fermion loop contribution. Therefore the flows of $Z^{\parallel}$ and $Z^{\perp}$ are mostly dominated by the fermionic contributions in (2.7) and (2.8). Now we are ready to interpret **(a)**–**(c)** above.

At high temperature, fermions acquire a large screening mass $q_4 \sim \pi T$ due to the antiperiodic boundary condition along the x^4 direction. Then the fermionic contribution to (2.7) and (2.8) is strongly suppressed and consequently $Z_k^{\parallel}$ and $Z_k^{\perp}$ almost cease to flow. Indeed, $Z_{k=0}^{\perp} \simeq 0.265$ at $T/T_{\rm pc} = 2$, which is close to the initial value, $Z_{k=\Lambda}^{\perp} = 0.236$. Thus we expect that both $Z^{\parallel}$ and $Z^{\perp}$ tend to their initial values at sufficiently high temperature. This should be true in a magnetic field, too, as long as $\sqrt{eB}$ does not exceed the screening scale $\sim \pi T$. This is an intuitive explanation to **(a)**.

As for **(b)**, the increase of $Z^{\parallel}$ is most likely attributable to the enhancement of the lowest Landau level ($n = 0$) contribution in (2.8). The contribution from the higher Landau levels is clearly suppressed for large $|eB|$ and they decouple from the flow of $Z_k^{\parallel}$.

Let us finally turn to **(c)**. The weak dependence of $Z^{\perp}$ on the magnetic field, in stark contrast to $Z^{\parallel}$, is quite natural in view of the fact that the flow of $Z^{\perp}$, (2.7), has no explicit dependence on $|eB|$. (This fact itself is a result of complicated nontrivial cancellations of $|eB|$-dependence among infinite series, as demonstrated in the appendix B.2.1.) The slight decrease of $Z^{\perp}$ as a function of $|eB|$ is more subtle; we speculate that this tendency originates from the enhancement of the constituent quark mass in a magnetic field (cf. Fig. 1). Because $\overline{\rho}_k$ grows with $|eB|$ owing to the magnetic catalysis, the fermionic contribution in (2.7) is suppressed, and the growth of $Z_k^{\perp}$ toward $k = 0$ is slowed down. Thus the decrease of $Z_{k=0}^{\perp}$ seems to be a natural consequence of large $|eB|$.

The ratio of $Z^{\perp}$ to $Z^{\parallel}$ gives the squared transverse velocity, $v_{\perp}^2$. Even at $eB = 0$, $v_{\perp}^2$

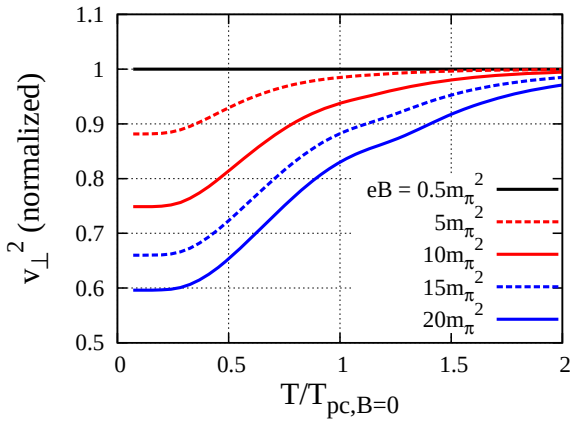


Figure 5. Squared transverse velocity $v_\perp^2 = Z^\perp/Z^\parallel$ with varying external magnetic field. The velocity is normalized by that at $eB = 0.5m_\pi^2$.

deviates from 1 owing to the finite temperature effect. To see the effect of the external magnetic field, it is convenient to normalize $v_\perp^2$ by that at $eB = 0.5m_\pi^2$. In Fig. 5 we show the temperature dependence of $v_\perp^2$ thus normalized for varying external magnetic field. For all temperatures, the velocity decreases with eB. This behavior is consistent with previous works that studied neutral mesons at $T = 0$ [10, 11, 55]. Our new finding here is that $v_\perp$ has a strong temperature dependence: at high temperature ($\gtrsim T_{\rm pc}$) even the magnetic field as strong as $20m_\pi^2$ does not modify $v_\perp^2$ significantly. This tendency can naturally be understood by recalling the temperature dependence of $Z^\parallel$ and $Z^\perp$ (cf. **(a)**). Therefore the "dimensional reduction" of neutral mesons is unlikely to modify the nature of the chiral crossover in a qualitative way.

In Fig. 6 (top), we show the renormalized pion masses obtained in full FRG. As remarked in section 2.4, the screening masses acquire a directional dependence in a strong magnetic field.[7] For comparison, in Fig. 6 (bottom) we also present the pion mass from LPA. In all three cases, we observe that the neutral pion mass *decreases* in a magnetic field. This trend is consistent with lattice simulations [45, 76], chiral perturbation theory [77–80], and an analytical study [81].

Furthermore, by comparing full FRG with LPA we find that $m_\pi^\parallel$ and $m_\pi^\perp$ grow more steeply with T than m_π in LPA for $T \gtrsim T_{\rm pc}$. This difference originates from the fact that $Z^\parallel$ and $Z^\perp$ decrease rapidly with T (cf. Fig. 4). Because of this rapid growth of the pion pole mass in full FRG at high T, the mesonic contributions to the flow are suppressed as compared to LPA. Therefore it is natural that in Fig. 3 the pseudo-critical temperature of full FRG shows the same trend with the mean-field approximation rather than LPA.

In Fig. 7, we present temperature dependence of the renormalized longitudinal and transverse pion decay constants (see (2.26) and (2.27) for their definitions). At each temperature, both pion decay constants increase with eB, but with different rates. Because $Z^\parallel$ increases with the external magnetic field, it enhances the increase of $f_\pi^{\rm bare}$. On the other

[7] Within our truncation the pole mass and the longitudinal screening mass are identical, although they can be different in QCD at finite temperature.

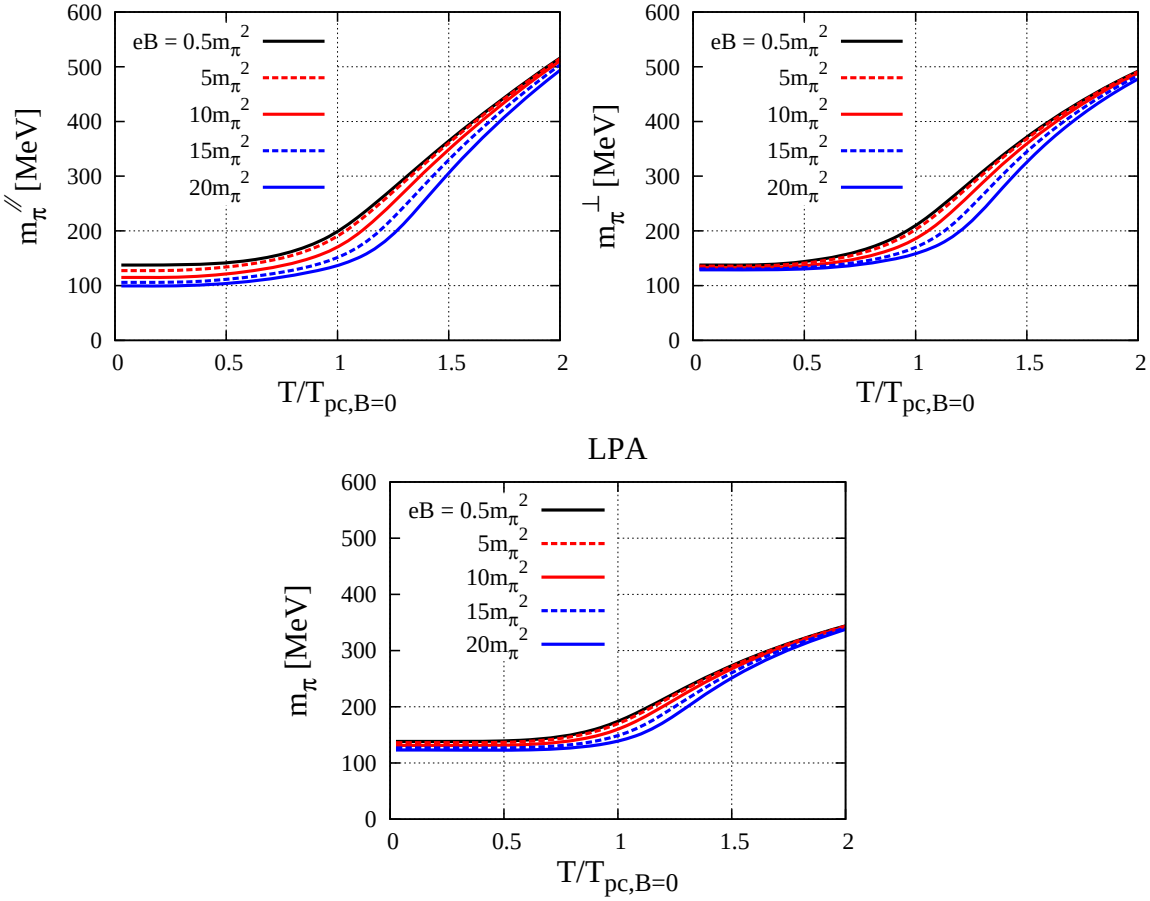


Figure 6. The longitudinal (top, left) and transverse (top, right) pion screening masses from full FRG, and the pion mass from LPA (bottom), with varying external magnetic field.

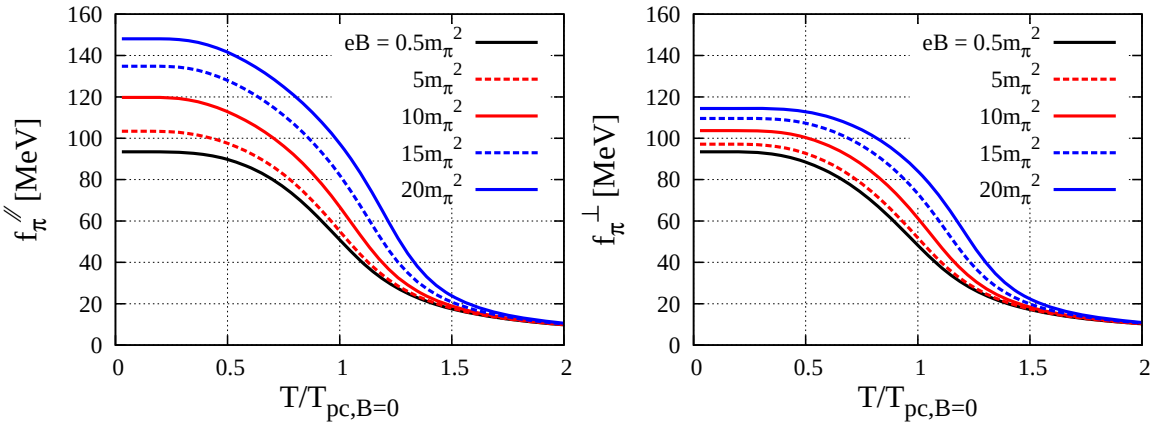


Figure 7. The longitudinal (left) and transverse (right) pion decay constants for varying external magnetic field.

hand, $Z^{\perp}$ decreases with the external field. Then the increase of $f_{\pi}^{\rm bare}$ is partially canceled by $Z_{\perp}$. However the decrease of $Z_{\perp}$ is not rapid enough to decrease $f_{\pi}^{\perp}$ with the external magnetic field.

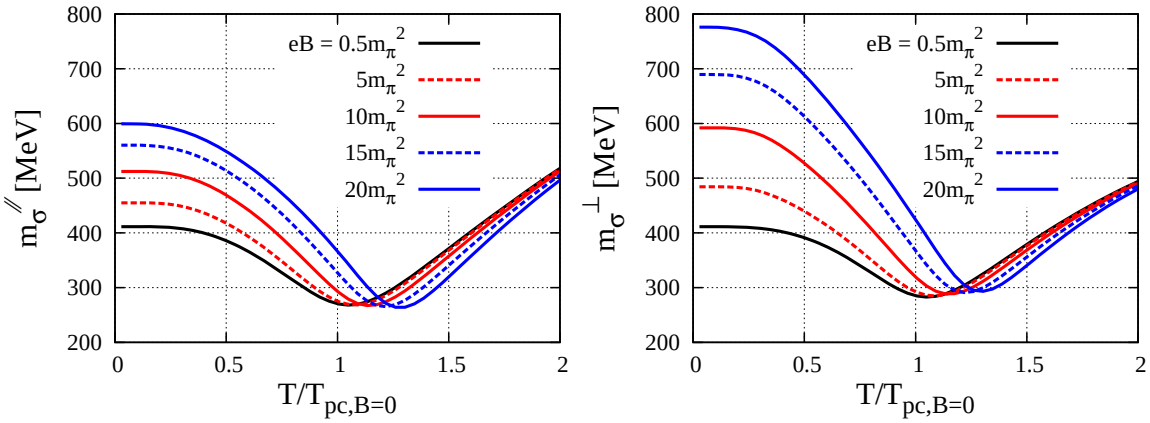


Figure 8. The longitudinal (left) and transverse (right) sigma screening masses with varying external magnetic field.

Finally, in Fig. 8, we show the direction-dependent renormalized screening masses of the sigma meson. Both sigma masses have minimums near the critical temperature. Above $T_{\rm pc}$, the pion and sigma masses for each direction are almost degenerate, signaling the effective restoration of chiral symmetry.

Below $T_{\rm pc}$, $m_\pi^{\parallel}$ and $m_\sigma^{\perp}$ are far more sensitive to the external magnetic field than $m_\pi^{\perp}$ and $m_\sigma^{\parallel}$. The reason is as follows. The bare pion mass decreases with the external magnetic field while the bare sigma mass increases. On the other hand, $Z^{\parallel}$ increases and $Z^{\perp}$ decreases with the external magnetic field, respectively. As for $m_\pi^{\parallel}$ and $m_\sigma^{\perp}$, the wave function renormalization and the bare meson masses conspire to increase the renormalized masses. Regarding $m_\pi^{\perp}$ and $m_\sigma^{\parallel}$, the effects of the wave function renormalization and the bare meson masses interfere with each other and the resulting change in the screening mass is reduced.

Above $T_{\rm pc}$, both the wave function renormalizations and the bare meson masses become less sensitive to the external magnetic field. Then the renormalized screening masses also become insensitive to the external magnetic field.

4 Conclusion

In the present work, we have examined influences of the external magnetic field on the chiral symmetry breaking of strongly interacting matter. In order to elucidate the dynamics of neutral mesons in the simplest possible setting, we have solved the quark-meson model with one light flavor. The quantum and thermal fluctuations of mesons and quarks were incorporated with the method of the functional renormalization group (FRG) equation.

We have carried out the derivative expansion of the average effective action up to second order in the mesonic momentum. With this extended truncation, we have successfully taken into account a spatial anisotropy of the neutral meson modes which is induced through their coupling to quarks. Although this effect has not been considered in previous FRG studies [27–30, 35], it is expected to be the origin of the inverse magnetic catalysis [55] and our work is the first attempt to test this conjecture using FRG. By devising a novel regulator

that is suitable for analysis in a magnetic field, we have derived flow equations for the scale-dependent effective potential and the wave function renormalization at finite temperature and external magnetic field. Then we have solved the flow equations numerically using the Taylor expansion method, and compared the obtained results with those from the leading-order derivative expansion (the so-called LPA) and the conventional mean-field approximation.

Our main findings are as follows.

- ⋆ At all temperatures, the constituent quark mass increases with the external magnetic field. Accordingly, the pseudo-critical temperature $T_{\rm pc}$ of chiral restoration is found to increase linearly with the magnetic field. The slope of $T_{\rm pc}$ is close to the mean-field value. We gave a microscopic explanation to this result based on the structure of the flow equations.
- ⋆ The velocity $v_\perp$ of the neutral mesons moving perpendicular to the magnetic field is found to decrease with the magnetic field at all temperatures, with the largest reduction in $v_\perp$ being observed at zero temperature. In contrast, at high temperature $\gtrsim T_{\rm pc}$, $v_\perp$ becomes rather insensitive to the magnetic field.
- ⋆ We computed the pion decay constants and the screening masses of the neutral mesons for the parallel and perpendicular directions to the external magnetic field. Below $T_{\rm pc}$ they show a large directional dependence, reflecting the anisotropy of the wave function renormalizations.

Finally we comment on possible future directions. First and foremost, the behavior of $T_{\rm pc}$ in this work is not qualitatively consistent with the lattice simulation performed at the physical point [43, 46], and we must seek for a proper explanation of the inverse magnetic catalysis, e.g., in the dynamics of gluons which were not taken into account in this work. Indeed the importance of the Polyakov loop was underlined in [57]. However the preceding analyses [21, 27, 35, 82] seem to suggest that just adding the Polyakov loop in a phenomenological way does not resolve the discrepancy with the lattice data. One way to address this problem within FRG would be to start from the QCD Lagrangian itself rather than effective models.

It would be also interesting to extend our Ansatz of the effective action to two flavors, so that the dynamics of charged mesons is taken into account. From a technical point of view, it is desirable to find a more useful regulator function that does not break the rotational symmetry explicitly. Finally, to make contact with experiments and observations, we should allow for a time-dependent magnetic field and evaluate its impact on chiral dynamics. We leave these issues for future work.

Acknowledgments

We are grateful to T. Hatsuda, Y. Hidaka and J. Pawlowski for useful discussions. KK was supported by the Special Postdoctoral Research Program of RIKEN. TK was supported by RIKEN iTHES Project and JSPS KAKENHI Grants Number 25887014.

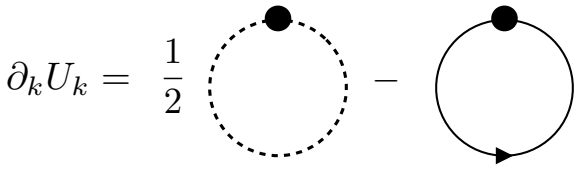


Figure 9. Diagrammatic representation of the flow equation (A.1). The dashed line (the solid line with arrow) represents a scale-dependent meson (fermion) propagator, respectively. The black blob stands for the insertion of $\partial_k R_k$.

A Derivation of the flow equation for U_k

In this appendix we will give a detailed derivation of (2.6). First of all, in a purely bosonic constant background, the effective action is related to the effective potential as $\Gamma_k/V_4 = U_k(\rho) - h\sigma$ where $V_4 \equiv \beta L^3$ denotes the Euclidean space-time volume. Consequently, from (2.1), the flow equation for the effective potential is obtained as

$$\partial_k U_k = \frac{1}{V_4}\left\{ \underbrace{\frac{1}{2}\,\mathrm{Tr}\left[\frac{1}{\Gamma_k^{(2,0)} + R_k^B}\partial_k R_k^B\right]}_{\text{bosons}} - \underbrace{\mathrm{Tr}\left[\frac{1}{\Gamma_k^{(0,2)} + R_k^F}\partial_k R_k^F\right]}_{\text{fermions}} \right\}. \tag{A.1}$$

The corresponding diagrams are shown in Fig. 9. We note that the dependence of U_k on the magnetic field entirely comes from the second term, because the bosons carry no electric charge. The bosonic contribution and the fermionic contribution will be evaluated in the appendices A.1 and A.2, respectively.

A.1 Bosonic contribution to $\partial_k U_k$

From (A.1) and (2.2), we get

$$\partial_k U_k\Big|_{\text{bose}} = \frac{1}{2}\,\mathrm{Tr}\left[\frac{1}{\Gamma_k^{(2,0)} + R_k^B}\partial_k R_k^B\right]/V_4 \tag{A.2}$$

$$= \frac{1}{2}\,\mathrm{Tr}\left[\frac{1}{-Z_k^{\parallel}(\partial_4^2+\partial_3^2) - Z_k^{\perp}(\partial_1^2+\partial_2^2) + R_k^B + U_k'(\rho)}\partial_k R_k^B\right]/V_4$$
$$+ \frac{1}{2}\,\mathrm{Tr}\left[\frac{1}{-Z_k^{\parallel}(\partial_4^2+\partial_3^2) - Z_k^{\perp}(\partial_1^2+\partial_2^2) + R_k^B + U_k'(\rho) + 2\rho U_k''(\rho)}\partial_k R_k^B\right]/V_4 \tag{A.3}$$

$$= \frac{1}{2}\,T\sum_{p_4:\,\text{even}}\int\frac{d^3p}{(2\pi)^3}\left\{(k^2-p_3^2)\partial_k Z_k^{\parallel} + 2kZ_k^{\parallel}\right\}\theta(k^2-p_3^2)$$
$$\times\left[\frac{1}{Z_k^{\parallel}(p_4^2+k^2) + Z_k^{\perp}p_\perp^2 + U_k'(\rho)} + \frac{1}{Z_k^{\parallel}(p_4^2+k^2) + Z_k^{\perp}p_\perp^2 + U_k'(\rho) + 2\rho U_k''(\rho)}\right] \tag{A.4}$$

$$= k^2\left(1 + \frac{k}{3}\frac{\partial_k Z_k^{\parallel}}{Z_k^{\parallel}}\right)\int'\frac{d^2p_\perp}{(2\pi)^3}\left(\frac{1}{E_\pi(\rho)}\coth\frac{E_\pi(\rho)}{2T} + \frac{1}{E_\sigma(\rho)}\coth\frac{E_\sigma(\rho)}{2T}\right), \tag{A.5}$$

with $p_\perp \equiv (p_1, p_2)$. The definitions of $E_\pi(\rho)$ and $E_\sigma(\rho)$ are given in (2.11).

A.2 Fermionic contribution to $\partial_k U_k$

From (A.1) and (2.3), we get

$$\partial_k U_k\Big|_{\text{fermi}} = -\operatorname{Tr}\left[\frac{1}{\Gamma_k^{(0,2)} + R_k^F}\partial_k R_k^F\right]/V_4 \tag{A.6}$$

$$= -N_c \operatorname{Tr}\left[\frac{1}{\not\partial_4 + (\not\partial_3 + R_k^F) + \not D_\perp + g(\sigma + i\gamma_5\pi)}\partial_k R_k^F\right]/V_4 \qquad (\not D_\perp \equiv \gamma_1 D_1 + \gamma_2 D_2) \tag{A.7}$$

$$= -N_c \operatorname{Tr}\left[\frac{\not\partial_3 + R_k^F}{\partial_4^2 + (\not\partial_3 + R_k^F)^2 + \not D_\perp^2 - 2g^2\rho}\partial_k R_k^F\right]/V_4 \tag{A.8}$$

$$= -N_c\, T\sum_{p_4:\,\text{odd}} \int \frac{dp_3}{2\pi} \operatorname{Tr}\left[\frac{-i\not p_3 \dfrac{k}{|p_3|}}{-p_4^2 - k^2 + \not D_\perp^2 - 2g^2\rho}\frac{-i\not p_3}{|p_3|}\theta(k^2 - p_3^2)\right]/L^2 \tag{A.9}$$

$$= -\frac{1}{\pi}N_c k^2\, T\sum_{p_4:\,\text{odd}} \operatorname{Tr}\left[\frac{1}{p_4^2 + k^2 - \not D_\perp^2 + 2g^2\rho}\right]/L^2\,. \tag{A.10}$$

The trace can be evaluated using the eigenfunctions of $\not D_\perp^2$, with the result

$$\partial_k U_k\Big|_{\text{fermi}} = -\frac{2}{\pi}N_c k^2\, T\sum_{p_4:\,\text{odd}} \Big(\frac{|eB|}{2\pi}\sum_{n=0}^{\infty}\Big) \sum_{s=\pm 1/2} \frac{1}{p_4^2 + k^2 + (2n + 1 - 2s)|eB| + 2g^2\rho} \tag{A.11}$$

$$= -\frac{2}{\pi}N_c k^2 \frac{|eB|}{2\pi}{\sum_{n=0}^{\infty}}' \frac{\alpha_n}{2E_n(\rho)} \tanh\frac{E_n(\rho)}{2T}\,, \tag{A.12}$$

with α_n and $E_n(\rho)$ defined in (2.10). The factor 2 in front of (A.11) stands for the degeneracy of eigenvalues of $\not D_\perp^2$ arising from the symmetry $[\not D_\perp^2, \gamma_5] = 0$. As a check, we also computed $\partial_k U_k\Big|_{\text{fermi}}$ using the fermion propagator in a magnetic field (B.51) and found that the result agrees with (A.12) exactly, as it should.

Finally the sum of (A.12) and (A.5) yields $\partial_k U_k$ in (2.6).

B Derivation of the flow equations for $Z_k^\perp$ and $Z_k^\parallel$

The flow of $Z_k^\perp$ and $Z_k^\parallel$ receives contribution from the diagrams in Fig. 10. We shall evaluate the meson-loop diagram in appendix B.1 and the fermion-loop diagram in appendix B.2. For brevity we use shorthand notations

$$\int_x \equiv \int_0^\beta dx_4 \int d^3x \qquad \text{and} \qquad \int_p \equiv T\sum_{p_4}\int \frac{d^3p}{(2\pi)^3}\,. \tag{B.1}$$

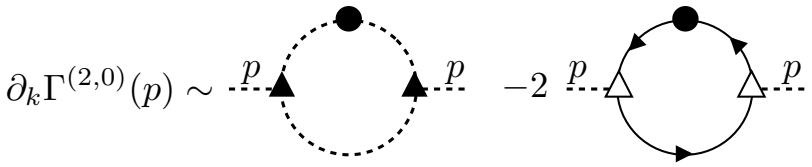


Figure 10. Diagrammatic representation of the flow equation for the mesonic two-point function. The dashed line (the solid line with arrow) represents a scale-dependent meson (fermion) propagator, respectively. The black blob stands for the insertion of $\partial_k R_k$. (Another one-loop diagram with a single four-meson vertex is not shown here as it does not contribute to the wave function renormalization.)

B.1 Bosonic contribution to $\partial_k Z_k$

Let us denote by $\tilde{\partial}_k$ a derivative that only acts on the k-dependence of the regulator R_k^B. With (2.1) and R_k^B in (2.2), the contribution of bosons to the flow equation is found to be

$$\partial_k\Gamma_k\Big|_{\text{bose}} = \frac{1}{2}\tilde{\partial}_k \,\mathrm{Tr}\log[\Gamma_k^{(2,0)} + R_k^B] \tag{B.2}$$

$$= \frac{1}{2}\tilde{\partial}_k \,\mathrm{Tr}\log\left[\underbrace{-Z_k^{\perp}(\partial_1^2+\partial_2^2) - Z_k^{\parallel}(\partial_3^2+\partial_4^2) + R_k^B}_{\equiv\, H_k} + \begin{pmatrix} \frac{\partial^2 U_k}{\partial\sigma^2} & \frac{\partial^2 U_k}{\partial\sigma\partial\pi} \\ \frac{\partial^2 U_k}{\partial\pi\partial\sigma} & \frac{\partial^2 U_k}{\partial\pi^2} \end{pmatrix}\right] \tag{B.3}$$

$$= \frac{1}{2}\tilde{\partial}_k \,\mathrm{Tr}\log\left[H_k + \begin{pmatrix} U_k'(\rho)+U_k''(\rho)\sigma^2 & U_k''(\rho)\sigma\pi \\ U_k''(\rho)\sigma\pi & U_k'(\rho)+U_k''(\rho)\pi^2 \end{pmatrix}\right]. \tag{B.4}$$

We evaluate this in the background $(\sigma,\pi) = (\overline{\sigma}_k, t(x))$ where $\overline{\sigma}_k$ is the running minimum of the potential: $\overline{\sigma}_k \equiv \underset{\sigma}{\mathrm{argmin}}\left\{U_k(\rho) - h\sigma\right\}$. Then $\rho = \frac{1}{2}\overline{\sigma}_k^2 + \frac{1}{2}t^2 \equiv \overline{\rho}_k + \frac{1}{2}t^2$. Therefore

$$\partial_k\Gamma_k\Big|_{\text{bose}}\Big|_{O(t^2)}$$

$$= \frac{1}{2}\tilde{\partial}_k \,\mathrm{Tr}\log\left[H_k + \begin{pmatrix} U_k'(\overline{\rho}_k+\frac{t^2}{2}) + 2\overline{\rho}_k U_k''(\overline{\rho}_k+\frac{t^2}{2}) & U_k''(\overline{\rho}_k+\frac{t^2}{2})\overline{\sigma}_k t \\ U_k''(\overline{\rho}_k+\frac{t^2}{2})\overline{\sigma}_k t & U_k'(\overline{\rho}_k+\frac{t^2}{2}) + U_k''(\overline{\rho}_k+\frac{t^2}{2})t^2 \end{pmatrix}\right]\Bigg|_{O(t^2)} \tag{B.5}$$

$$= \frac{1}{2}\tilde{\partial}_k \,\mathrm{Tr}\log\left[A+B+C\right]\Big|_{O(t^2)} \tag{B.6}$$

$$= \frac{1}{2}\tilde{\partial}_k \,\mathrm{Tr}\left[A^{-1}C - \frac{1}{2}A^{-1}BA^{-1}B\right], \tag{B.7}$$

with the definitions

$$A \equiv \begin{pmatrix} H_k + U_k'(\overline{\rho}_k) + 2\overline{\rho}_k U_k''(\overline{\rho}_k) & 0 \\ 0 & H_k + U_k'(\overline{\rho}_k) \end{pmatrix} \equiv \begin{pmatrix} H_k + \hat{m}_\sigma^2 & 0 \\ 0 & H_k + \hat{m}_\pi^2 \end{pmatrix}, \tag{B.8}$$

$$B \equiv \begin{pmatrix} 0 & U_k''(\overline{\rho}_k)\overline{\sigma}_k t \\ U_k''(\overline{\rho}_k)\overline{\sigma}_k t & 0 \end{pmatrix}, \tag{B.9}$$

$$C \equiv \begin{pmatrix} \frac{1}{2}U_k''(\overline{\rho}_k)t^2 + \overline{\rho}_k U_k'''(\overline{\rho}_k)t^2 & 0 \\ 0 & \frac{3}{2}U_k''(\overline{\rho}_k)t^2 \end{pmatrix}. \tag{B.10}$$

The first term in (B.7) can be neglected as it does not generate a kinetic term $\sim t_p t_{-p}$. As for the second term,

$$\frac{1}{2}\tilde{\partial}_k \,\mathrm{Tr}\left[-\frac{1}{2}A^{-1}BA^{-1}B\right] = -\overline{\rho}_k\big[U_k''(\overline{\rho}_k)\big]^2\tilde{\partial}_k\,\mathrm{Tr}\left[A_{11}^{-1}tA_{22}^{-1}t\right] \tag{B.11}$$

$$= -\overline{\rho}_k\big[U_k''(\overline{\rho}_k)\big]^2\tilde{\partial}_k\int_{pq}(A_{11}^{-1})_p t_{p-q}(A_{22}^{-1})_q t_{q-p} \tag{B.12}$$

$$= -\overline{\rho}_k\big[U_k''(\overline{\rho}_k)\big]^2\tilde{\partial}_k\int_p t_p t_{-p}\int_q (A_{11}^{-1})_{p+q}(A_{22}^{-1})_q\,. \tag{B.13}$$

On the other hand, we have

$$\partial_k\Gamma_k = \partial_k\int_x\Big\{\frac{Z_k^\perp}{2}\sum_{i=1,2}(\partial_i t)^2 + \frac{Z_k^\parallel}{2}\sum_{i=3,4}(\partial_i t)^2 + \dots\Big\} \tag{B.14}$$

$$= \frac{1}{2}\partial_k Z_k^\perp\int_p t_p t_{-p}(p_1^2+p_2^2) + \frac{1}{2}\partial_k Z_k^\parallel\int_p t_p t_{-p}(p_3^2+p_4^2) + \dots\,. \tag{B.15}$$

Comparing (B.15) with (B.13), we are led to the important formulae

$$\partial_k Z_k^\perp\Big|_{\text{bose}} = -\overline{\rho}_k\big[U_k''(\overline{\rho}_k)\big]^2\lim_{p\to 0}\frac{\partial^2}{\partial p_1^2}\tilde{\partial}_k\int_q (A_{11}^{-1})_{p+q}(A_{22}^{-1})_q\,, \tag{B.16}$$

$$\partial_k Z_k^\parallel\Big|_{\text{bose}} = -\overline{\rho}_k\big[U_k''(\overline{\rho}_k)\big]^2\lim_{p\to 0}\frac{\partial^2}{\partial p_3^2}\tilde{\partial}_k\int_q (A_{11}^{-1})_{p+q}(A_{22}^{-1})_q\,. \tag{B.17}$$

Without loss of generality one can assume $p=(p_1,0,p_3,0)$. With a bit of algebra, we find

$$\tilde{\partial}_k\int_q (A_{11}^{-1})_{\hat{p}}(A_{22}^{-1})_q\Big|_{\hat{p}=q+p}$$

$$= \tilde{\partial}_k\int_q \frac{1}{Z_k^\perp(\hat{p}_1^2+\hat{p}_2^2)+Z_k^\parallel(\hat{p}_3^2+\hat{p}_4^2)+R_k^B(\hat{p})+\hat{m}_\sigma^2}\;\frac{1}{Z_k^\perp(q_1^2+q_2^2)+Z_k^\parallel(q_3^2+q_4^2)+R_k^B(q)+\hat{m}_\pi^2}\Big|_{\hat{p}=q+p} \tag{B.18}$$

$$= -T\sum_{q_4:\,\text{even}}\Big\{I(Z_k^\parallel q_4^2+\hat{m}_\sigma^2, Z_k^\parallel q_4^2+\hat{m}_\pi^2; p) + (\hat{m}_\sigma^2\leftrightarrow\hat{m}_\pi^2)\Big\}, \tag{B.19}$$

with

$$I(\zeta,\zeta';p)\equiv$$

$$\int\frac{d^3q}{(2\pi)^3}\frac{\big[2kZ_k^\parallel+(k^2-q_3^2)\partial_k Z_k^\parallel\big]\,\theta(k^2-q_3^2)}{\big[Z_k^\perp(q_1^2+q_2^2)+Z_k^\parallel k^2+\zeta\big]^2\Big\{Z_k^\perp\big((q_1-p_1)^2+q_2^2\big)+Z_k^\parallel(q_3-p_3)^2+R_k^B(q-p)+\zeta'\Big\}}\,. \tag{B.20}$$

The next task is to extract the $O(p^2)$ part of $I(\zeta,\zeta';p)$. To take care of $R_k^B(q-p)$ in the denominator, we decompose this integral into two pieces as $I(\zeta,\zeta';p) = I_1(\zeta,\zeta';p) +$

$I_2(\zeta,\zeta';p)$, with

$$I_1(\zeta,\zeta';p) \equiv$$
$$\int \frac{d^3q}{(2\pi)^3} \frac{\left[2kZ_k^{\parallel} + (k^2-q_3^2)\partial_k Z_k^{\parallel}\right]\theta(k^2-q_3^2)\;\theta\big(k^2-(q_3-p_3)^2\big)}{\left[Z_k^{\perp}(q_1^2+q_2^2)+Z_k^{\parallel}k^2+\zeta\right]^2\Big\{Z_k^{\perp}\big((q_1-p_1)^2+q_2^2\big)+Z_k^{\parallel}(q_3-p_3)^2+R_k^B(q-p)+\zeta'\Big\}}\,, \tag{B.21}$$

$$I_2(\zeta,\zeta';p) \equiv$$
$$\int \frac{d^3q}{(2\pi)^3} \frac{\left[2kZ_k^{\parallel} + (k^2-q_3^2)\partial_k Z_k^{\parallel}\right]\theta(k^2-q_3^2)\;\big\{1-\theta\big(k^2-(q_3-p_3)^2\big)\big\}}{\left[Z_k^{\perp}(q_1^2+q_2^2)+Z_k^{\parallel}k^2+\zeta\right]^2\Big\{Z_k^{\perp}\big((q_1-p_1)^2+q_2^2\big)+Z_k^{\parallel}(q_3-p_3)^2+R_k^B(q-p)+\zeta'\Big\}}\,, \tag{B.22}$$

A straightforward but tedious calculation yields

$$\lim_{p\to0}\frac{\partial^2}{\partial p_1^2} I_1(\zeta,\zeta';p) =$$
$$-16k^2\big(Z_k^{\perp}\big)^2\left(Z_k^{\parallel}+\frac{k}{3}\partial_k Z_k^{\parallel}\right)\int\frac{d^2q_{\perp}}{(2\pi)^3}\frac{q_{\perp}^2}{(Z_k^{\perp}q_{\perp}^2+Z_k^{\parallel}k^2+\zeta)^3(Z_k^{\perp}q_{\perp}^2+Z_k^{\parallel}k^2+\zeta')^2}\,, \tag{B.23}$$

$$\lim_{p\to0}\frac{\partial^2}{\partial p_3^2} I_1(\zeta,\zeta';p) = -2k\partial_k Z_k^{\parallel}\int\frac{d^2q_{\perp}}{(2\pi)^3}\frac{1}{(Z_k^{\perp}q_{\perp}^2+Z_k^{\parallel}k^2+\zeta)^2(Z_k^{\perp}q_{\perp}^2+Z_k^{\parallel}k^2+\zeta')}\,, \tag{B.24}$$

$$\lim_{p\to0}\frac{\partial^2}{\partial p_1^2} I_2(\zeta,\zeta';p) = 0\,, \tag{B.25}$$

$$\lim_{p\to0}\frac{\partial^2}{\partial p_3^2} I_2(\zeta,\zeta';p) =$$
$$\int\frac{d^2q_{\perp}}{(2\pi)^3}\frac{1}{(Z_k^{\perp}q_{\perp}^2+Z_k^{\parallel}k^2+\zeta)^2}\left(-\frac{4k^2(Z_k^{\parallel})^2}{(Z_k^{\perp}q_{\perp}^2+Z_k^{\parallel}k^2+\zeta')^2}+\frac{2k\partial_k Z_k^{\parallel}}{Z_k^{\perp}q_{\perp}^2+Z_k^{\parallel}k^2+\zeta'}\right). \tag{B.26}$$

Combining all the above and performing a change of variable ($q_{\perp}^2 \to \frac{Z_k^{\parallel}}{Z_k^{\perp}}q_{\perp}^2$), we get

$$\lim_{p\to0}\frac{\partial^2}{\partial p_1^2} I(\zeta,\zeta';p) = -16\frac{k^2}{(Z_k^{\parallel})^2}\left(1+\frac{k}{3}\frac{\partial_k Z_k^{\parallel}}{Z_k^{\parallel}}\right)\int\frac{d^2q_{\perp}}{(2\pi)^3}\frac{q_{\perp}^2}{\left(q_{\perp}^2+k^2+\frac{\zeta}{Z_k^{\parallel}}\right)^3\left(q_{\perp}^2+k^2+\frac{\zeta'}{Z_k^{\parallel}}\right)^2} \tag{B.27}$$

$$= -\frac{2}{\pi^2}\frac{k^2}{(Z_k^{\parallel})^2}\left(1+\frac{k}{3}\frac{\partial_k Z_k^{\parallel}}{Z_k^{\parallel}}\right)\int_0^{\infty}dw\frac{w}{\left(w+k^2+\frac{\zeta}{Z_k^{\parallel}}\right)^3\left(w+k^2+\frac{\zeta'}{Z_k^{\parallel}}\right)^2}\,, \tag{B.28}$$

$$\lim_{p\to0}\frac{\partial^2}{\partial p_3^2} I(\zeta,\zeta';p) = -4\frac{k^2}{Z_k^{\parallel}Z_k^{\perp}}\int\frac{d^2q_{\perp}}{(2\pi)^3}\frac{1}{\left(q_{\perp}^2+k^2+\frac{\zeta}{Z_k^{\parallel}}\right)^2\left(q_{\perp}^2+k^2+\frac{\zeta'}{Z_k^{\parallel}}\right)^2} \tag{B.29}$$

$$= -\frac{1}{2\pi^2}\frac{k^2}{Z_k^{\parallel}Z_k^{\perp}}\int_0^{\infty}\frac{dw}{\left(w+k^2+\frac{\zeta}{Z_k^{\parallel}}\right)^2\left(w+k^2+\frac{\zeta'}{Z_k^{\parallel}}\right)^2}\,. \tag{B.30}$$

Plugging these into (B.16) and (B.17), we find

$$\begin{aligned}
&\partial_k Z_k^{\perp}\Big|_{\text{bose}} \\
&= \overline{\rho}_k \big[U_k''(\overline{\rho}_k)\big]^2 T \sum_{q_4:\,\text{even}} \lim_{p\to 0} \frac{\partial^2}{\partial p_1^2} \Big\{ I(Z_k^{\parallel} q_4^2 + \hat{m}_\sigma^2, Z_k^{\parallel} q_4^2 + \hat{m}_\pi^2; p) + (\hat{m}_\sigma^2 \leftrightarrow \hat{m}_\pi^2) \Big\} \qquad \text{(B.31)} \\
&= -\frac{k^2}{\pi^2} \frac{\overline{\rho}_k \big[U_k''(\overline{\rho}_k)\big]^2}{(Z_k^{\parallel})^2} \left(1 + \frac{k}{3} \frac{\partial_k Z_k^{\parallel}}{Z_k^{\parallel}}\right) T \sum_{q_4:\,\text{even}} \int_0^\infty \frac{dw}{\left(w + k^2 + q_4^2 + \frac{\hat{m}_\sigma^2}{Z_k^{\parallel}}\right)^2 \left(w + k^2 + q_4^2 + \frac{\hat{m}_\pi^2}{Z_k^{\parallel}}\right)^2}, \qquad \text{(B.32)}
\end{aligned}$$

and

$$\begin{aligned}
&\partial_k Z_k^{\parallel}\Big|_{\text{bose}} \\
&= \overline{\rho}_k \big[U_k''(\overline{\rho}_k)\big]^2 T \sum_{q_4:\,\text{even}} \lim_{p\to 0} \frac{\partial^2}{\partial p_3^2} \Big\{ I(Z_k^{\parallel} q_4^2 + \hat{m}_\sigma^2, Z_k^{\parallel} q_4^2 + \hat{m}_\pi^2; p) + (\hat{m}_\sigma^2 \leftrightarrow \hat{m}_\pi^2) \Big\} \qquad \text{(B.33)} \\
&= -\frac{k^2}{\pi^2} \frac{\overline{\rho}_k \big[U_k''(\overline{\rho}_k)\big]^2}{Z_k^{\parallel} Z_k^{\perp}} T \sum_{q_4:\,\text{even}} \int_0^\infty \frac{dw}{\left(w + k^2 + q_4^2 + \frac{\hat{m}_\sigma^2}{Z_k^{\parallel}}\right)^2 \left(w + k^2 + q_4^2 + \frac{\hat{m}_\pi^2}{Z_k^{\parallel}}\right)^2}. \qquad \text{(B.34)}
\end{aligned}$$

In deriving (B.32) we have used a mathematical formula

$$\int_0^\infty dw \frac{w}{(w+\alpha)^3(w+\beta)^2} + \int_0^\infty dw \frac{w}{(w+\alpha)^2(w+\beta)^3} = \frac{1}{2}\int_0^\infty \frac{dw}{(w+\alpha)^2(w+\beta)^2} \qquad \text{(B.35)}$$

which holds for $\alpha > 0$ and $\beta > 0$.

The expressions (B.32) and (B.34) are not so useful for numerical analysis since they involve infinite sums as well as integrals over the whole real axis. One can simplify them by using Feynman's integral formula and then taking the Matsubara sums analytically:

$$\begin{aligned}
&T \sum_{q_4:\,\text{even}} \int_0^\infty \frac{dw}{\left(w + k^2 + q_4^2 + \frac{\hat{m}_\sigma^2}{Z_k^{\parallel}}\right)^2 \left(w + k^2 + q_4^2 + \frac{\hat{m}_\pi^2}{Z_k^{\parallel}}\right)^2} \\
&= T \sum_{q_4:\,\text{even}} \int_0^1 dx\; 6x(1-x) \int_0^\infty \frac{dw}{\left(w + k^2 + q_4^2 + \frac{x\hat{m}_\sigma^2 + (1-x)\hat{m}_\pi^2}{Z_k^{\parallel}}\right)^4} \qquad \text{(B.36)} \\
&= T \sum_{q_4:\,\text{even}} \int_0^1 dx\; 2x(1-x) \frac{1}{\left(k^2 + q_4^2 + \frac{x\hat{m}_\sigma^2 + (1-x)\hat{m}_\pi^2}{Z_k^{\parallel}}\right)^3} \qquad \text{(B.37)} \\
&= \int_0^1 dx\; 2x(1-x) \frac{\left(6T^2 + Q^2 \operatorname{csch}^2 \frac{Q}{2T}\right) \coth \frac{Q}{2T} + 3TQ \cdot \operatorname{csch}^2 \frac{Q}{2T}}{32 \cdot T^2 \cdot Q^5}, \qquad \text{(B.38)}
\end{aligned}$$

with

$$Q = Q(x) \equiv \sqrt{k^2 + \frac{x\hat{m}_\sigma^2 + (1-x)\hat{m}_\pi^2}{Z_k^{\parallel}}}. \qquad \text{(B.39)}$$

We used this expression in our actual numerical computation.

B.2 Fermionic contribution to $\partial_k Z_k$

From (2.1),

$$\partial_k \Gamma_k\Big|_{\text{fermi}} = -\tilde{\partial}_k \,\mathrm{Tr}\log[\Gamma_k^{(0,2)} + R_k^F] \tag{B.40}$$

$$= -N_c\,\tilde{\partial}_k \,\mathrm{Tr}\log[\not{D} + R_k^F + g(\sigma + i\gamma_5\pi)]\,. \tag{B.41}$$

As in the previous section, we evaluate this in an inhomogeneous background $(\sigma(x), \pi(x)) = (\overline{\sigma}_k, t(x))$, with $\overline{\sigma}_k$ the running minimum of the potential: $\overline{\sigma}_k \equiv \underset{\sigma}{\mathrm{argmin}} \left\{U_k(\rho) - h\sigma\right\}$. Then

$$\partial_k \Gamma_k\Big|_{\text{fermi}} = -N_c\,\tilde{\partial}_k \,\mathrm{Tr}\log[\not{D} + R_k^F + g\overline{\sigma}_k + ig\gamma_5 t]\,. \tag{B.42}$$

Introducing the regulator-dependent fermion propagator $G \equiv \dfrac{1}{\not{D} + R_k^F + g\overline{\sigma}_k}$ one can expand (B.42) to $O(t^2)$ to obtain

$$\partial_k \Gamma_k\Big|_{\text{fermi}}\Big|_{O(t^2)} = -\frac{1}{2} N_c g^2 \tilde{\partial}_k \,\mathrm{Tr}[G\gamma_5 t G\gamma_5 t] \tag{B.43}$$

$$= -\frac{1}{2} N_c g^2 \tilde{\partial}_k \,\mathrm{Tr}[\tilde{G}\gamma_5 t \tilde{G}\gamma_5 t] \tag{B.44}$$

$$= -\frac{1}{2} N_c g^2 \int_p t_p t_{-p}\; \tilde{\partial}_k \int_q \mathrm{tr}[\tilde{G}_{p+q}\gamma_5 \tilde{G}_q \gamma_5]\,, \tag{B.45}$$

where 'tr' is a trace over spinor indices, and $\tilde{G}$ is the *translationally invariant part* of G. This replacement is justified because the so-called Schwinger phase [83] in G drops out of the trace in (B.43).

Comparing (B.45) with (B.15) we obtain

$$\partial_k Z_k^{\perp}\Big|_{\text{fermi}} = -N_c g^2 \int_q \tilde{\partial}_k \lim_{p\to 0} \frac{d}{dp_1^2}\,\mathrm{tr}[\tilde{G}_{p+q}\gamma_5 \tilde{G}_q \gamma_5]\,, \tag{B.46}$$

$$\partial_k Z_k^{\parallel}\Big|_{\text{fermi}} = -N_c g^2 \int_q \tilde{\partial}_k \lim_{p\to 0} \frac{d}{dp_3^2}\,\mathrm{tr}[\tilde{G}_{p+q}\gamma_5 \tilde{G}_q \gamma_5]\,. \tag{B.47}$$

A closed expression for $\tilde{G}_p$ was derived in [83] in the absence of the regulator R_k^F (see also [11, 38]). The formula, after analytic continuation to the Euclidean space-time, reads

$$\tilde{G}_p\Big|_{R_k^F=0} = \frac{1}{\not{D} + g\overline{\sigma}_k}(p) \tag{B.48}$$

$$= 2\exp\left(-\frac{p_\perp^2}{|eB|}\right) \sum_{n=0}^{\infty} \frac{(-1)^n D_n(p)}{p_4^2 + p_3^2 + 2|eB|n + g^2\overline{\sigma}_k^2}\,, \tag{B.49}$$

with $p_\perp^2 \equiv p_1^2 + p_2^2$ and

$$D_n(p) \equiv \left[i(p_4\gamma_4 + p_3\gamma_3) + g\overline{\sigma}_k\right] \left\{L_n\left(\frac{2p_\perp^2}{|eB|}\right)\mathcal{P}_+ - L_{n-1}\left(\frac{2p_\perp^2}{|eB|}\right)\mathcal{P}_-\right\}$$

$$- 2i(p_1\gamma_1 + p_2\gamma_2) L_{n-1}^{(1)}\left(\frac{2p_\perp^2}{|eB|}\right)\,. \tag{B.50}$$

Here $\mathcal{P}_\pm \equiv \frac{1}{2}(\mathbb{1} \mp i\gamma_1\gamma_2)$ are the spin projectors[8] while $L_n(x)$ and $L_n^{(\alpha)}(x)$ are the (generalized) Laguerre polynomials. In what follows, we promise $L_n(x) = L_n^{(\alpha)}(x) \equiv 0$ for $n < 0$.

In the presence of the regulator R_k^F in (2.3) the propagator is modified as $(\not{D}+g\overline{\sigma}_k)^{-1} \to (\not{D} + R_k^F + g\overline{\sigma}_k)^{-1} = \big(- i\not{p}_3[1 + r_k(p_3)] + \dots \big)^{-1}$. It follows that one can incorporate R_k^F into the propagator by simply replacing p_3 with $p_3[1 + r_k(p_3)]$. Therefore we have

$$\tilde{G}_p = 2 \exp\left(-\frac{p_\perp^2}{|eB|}\right) \sum_{n=0}^{\infty} \frac{(-1)^n D_n^{(k)}(p)}{p_4^2 + p_3^2[1 + r_k(p_3)]^2 + 2|eB|n + g^2\overline{\sigma}_k^2}\,, \tag{B.51}$$

with $D_n^{(k)}(p) \equiv D_n\big(p_1, p_2, p_3[1 + r_k(p_3)], p_4\big)$.

Before proceeding, let us introduce shorthand notations for some useful quantities:

$$\mathbf{q}_3 \equiv q_3 + p_3\,, \tag{B.52}$$

$$F_n(q_4, q_3) \equiv q_4^2 + q_3^2[1 + r_k(q_3)]^2 + 2|eB|n + g^2\overline{\sigma}_k^2\,, \tag{B.53}$$

$$\mathbf{F}_0(q_4, q_3, \mathbf{q}_3) \equiv q_4^2 + \mathbf{q}_3 q_3[1 + r_k(\mathbf{q}_3)][1 + r_k(q_3)] + g^2\overline{\sigma}_k^2\,. \tag{B.54}$$

Our remaining task is to plug (B.51) into (B.46) and (B.47). As this is a lengthy calculation we divide this into a few smaller steps. Firstly, we have from (B.51)

$$\mathrm{tr}[\tilde{G}_{p+q}\gamma_5\tilde{G}_q\gamma_5] = \; 4\exp\left(-\frac{(q+p)_\perp^2 + q_\perp^2}{|eB|}\right) \sum_{m=0}^{\infty}\sum_{n=0}^{\infty} \frac{(-1)^{m+n}\,\mathrm{tr}\left[D_m^{(k)}(q+p)\gamma_5 D_n^{(k)}(q)\gamma_5\right]}{F_m(q_4, \mathbf{q}_3)F_n(q_4, q_3)}\,. \tag{B.55}$$

Without loss of generality we may assume $p = (p_1, 0, p_3, 0)$. With a bit of algebra, the trace in the numerator becomes

$$\begin{aligned}
&\mathrm{tr}\left[D_m^{(k)}(q+p)\gamma_5 D_n^{(k)}(q)\gamma_5\right] \\
&= 2\mathbf{F}_0(q_4, q_3, \mathbf{q}_3)\left\{ L_m\left(\frac{2(q+p)_\perp^2}{|eB|}\right) L_n\left(\frac{2q_\perp^2}{|eB|}\right) + L_{m-1}\left(\frac{2(q+p)_\perp^2}{|eB|}\right) L_{n-1}\left(\frac{2q_\perp^2}{|eB|}\right)\right\} \\
&\qquad + 16(q_\perp^2 + q_1p_1)L_{m-1}^{(1)}\left(\frac{2(q+p)_\perp^2}{|eB|}\right) L_{n-1}^{(1)}\left(\frac{2q_\perp^2}{|eB|}\right)\,,
\end{aligned} \tag{B.56}$$

and the integration over the transverse momenta yields

$$\begin{aligned}
&\int \frac{d^2q_\perp}{(2\pi)^2} \exp\left(-\frac{(q+p)_\perp^2 + q_\perp^2}{|eB|}\right) \mathrm{tr}\left[D_m^{(k)}(q+p)\gamma_5 D_n^{(k)}(q)\gamma_5\right] \\
&= \mathbf{F}_0(q_4, q_3, \mathbf{q}_3)\frac{|eB|}{4\pi}\,\mathrm{e}^{-W}(-W)^{m-n}\times \\
&\qquad \times \left\{ \frac{n!}{m!}\left[L_n^{(m-n)}(W)\right]^2 \theta(m, n \geq 0) + \frac{(n-1)!}{(m-1)!}\left[L_{n-1}^{(m-n)}(W)\right]^2 \theta(m, n \geq 1)\right\} \\
&\quad + \frac{|eB|^2}{\pi}\,\mathrm{e}^{-W}(-W)^{m-n}\frac{n!}{(m-1)!}L_{n-1}^{(m-n)}(W)L_n^{(m-n)}(W)\;\theta(m, n \geq 1)
\end{aligned} \tag{B.57}$$

[8]The relative sign is reversed owing to the Euclidean convention. In this work we are using Hermitian gamma matrices defined as $\{\gamma_\mu, \gamma_\nu\} = 2\delta_{\mu\nu}$ with $(\gamma_\mu)^\dagger = \gamma_\mu$.

where $W \equiv \dfrac{p_1^2}{2|eB|}$, and $\theta(\bullet)$ is defined as unity if $(\bullet)$ is true, and zero otherwise. In deriving (B.57) we have used two mathematical formulas:

$$\begin{aligned}
&\int \frac{d^2q_\perp}{(2\pi)^2} \exp\left(-\frac{(q+p)_\perp^2+q_\perp^2}{|eB|}\right) L_k\left(\frac{2q_\perp^2}{|eB|}\right) L_\ell\left(\frac{2(q+p)_\perp^2}{|eB|}\right) \\
&= \frac{|eB|}{8\pi}\frac{k!}{\ell!}\,\mathrm{e}^{-\frac{p_\perp^2}{2|eB|}}\left(-\frac{p_\perp^2}{2|eB|}\right)^{\ell-k}\left[L_k^{(\ell-k)}\left(\frac{p_\perp^2}{2|eB|}\right)\right]^2 \qquad \text{for} \quad k,\,\ell \geq 0\,,
\end{aligned} \tag{B.58}$$

and

$$\begin{aligned}
&\int \frac{d^2q_\perp}{(2\pi)^2} \exp\left(-\frac{(q+p)_\perp^2+q_\perp^2}{|eB|}\right) (q_\perp^2 + q_\perp\cdot p_\perp) L_{k-1}^{(1)}\left(\frac{2q_\perp^2}{|eB|}\right) L_{\ell-1}^{(1)}\left(\frac{2(q+p)_\perp^2}{|eB|}\right) \\
&= \frac{|eB|^2}{16\pi}\frac{k!}{\ell!}\,\mathrm{e}^{-\frac{p_\perp^2}{2|eB|}}\left(-\frac{p_\perp^2}{2|eB|}\right)^{\ell-k}\ell L_{k-1}^{(\ell-k)}\left(\frac{p_\perp^2}{2|eB|}\right) L_k^{(\ell-k)}\left(\frac{p_\perp^2}{2|eB|}\right) \qquad \text{for} \quad k,\,\ell \geq 1\,.
\end{aligned} \tag{B.59}$$

From (B.55) and (B.57) we obtain

$$\begin{aligned}
&\int \frac{d^2q_\perp}{(2\pi)^2}\,\mathrm{tr}[\tilde{G}_{p+q}\gamma_5\tilde{G}_q\gamma_5] \\
&= \frac{|eB|}{\pi}\mathbf{F}_0(q_4,q_3,\mathbf{q}_3)\sum_{m=0}^{\infty}\sum_{n=0}^{\infty}\frac{\mathrm{e}^{-W}W^{m-n}}{F_m(q_4,\mathbf{q}_3)F_n(q_4,q_3)}\times \\
&\qquad\times\left\{\frac{n!}{m!}\left[L_n^{(m-n)}(W)\right]^2 + \frac{(n-1)!}{(m-1)!}\left[L_{n-1}^{(m-n)}(W)\right]^2\theta(m,n\geq 1)\right\} \\
&\quad + \frac{4}{\pi}|eB|^2\sum_{m=1}^{\infty}\sum_{n=1}^{\infty}\frac{\mathrm{e}^{-W}W^{m-n}}{F_m(q_4,\mathbf{q}_3)F_n(q_4,q_3)}\frac{n!}{(m-1)!}L_{n-1}^{(m-n)}(W)L_n^{(m-n)}(W)\,.
\end{aligned} \tag{B.60}$$

From here on we shall consider $\partial_k Z_k^\perp\big|_{\text{fermi}}$ and $\partial_k Z_k^\parallel\big|_{\text{fermi}}$ separately.

B.2.1 Flow of $Z_k^\perp$

In the following we set $p_3 = 0$ without losing generality. Let us rewrite (B.46) as

$$\partial_k Z_k^\perp\Big|_{\text{fermi}} = -N_c g^2\, T\sum_{q_4:\,\text{odd}}\int\frac{dq_3}{2\pi}\,\tilde{\partial}_k\,\lim_{p\to 0}\frac{d}{dp_1^2}\int\frac{d^2q_\perp}{(2\pi)^2}\,\mathrm{tr}[\tilde{G}_{p+q}\gamma_5\tilde{G}_q\gamma_5] \tag{B.61}$$

$$= -N_c g^2\, T\sum_{q_4:\,\text{odd}}\int\frac{dq_3}{2\pi}\,\tilde{\partial}_k\left(\frac{1}{2|eB|}\lim_{W\to 0}\frac{d}{dW}\int\frac{d^2q_\perp}{(2\pi)^2}\,\mathrm{tr}[\tilde{G}_{p+q}\gamma_5\tilde{G}_q\gamma_5]\right). \tag{B.62}$$

We will carry out these operations in this order. First, recall that for $\alpha\in\mathbb{Z}$,

$$L_n^{(\alpha)}(x) \underset{x\to 0}{\sim} \begin{cases} \dbinom{n+\alpha}{n} & [\alpha\geq 0] \\ \dfrac{(-1)^\alpha}{(-\alpha)!}x^{-\alpha} & [-n\leq\alpha\leq -1] \\ (-1)^n\dbinom{-\alpha-1}{n} & [\alpha\leq -n-1] \end{cases}. \tag{B.63}$$

Using this, it is not difficult to show that all terms in (B.60) with $|m-n| \geq 2$ are $O(W^2)$ in the limit $W \to 0$ and do not contribute to (B.62). Therefore we obtain

$$\frac{1}{2|eB|} \lim_{W\to 0} \frac{d}{dW} \int \frac{d^2q_\perp}{(2\pi)^2} \operatorname{tr}[\tilde{G}_{p+q}\gamma_5 \tilde{G}_q \gamma_5] \tag{B.64}$$

$$= \frac{F_0(q_4,q_3)}{2\pi} \Big(\underbrace{g_1}_{m=n+1} + \underbrace{g_2}_{m=n-1} + \underbrace{g_3}_{m=n} \Big) + \frac{2|eB|}{\pi} \Big(\underbrace{g_4}_{m=n+1} + \underbrace{g_5}_{m=n-1} + \underbrace{g_6}_{m=n} \Big) , \tag{B.65}$$

where

$$g_1 = \sum_{n=0}^{\infty} \frac{2n+1}{F_{n+1}(q_4,q_3)F_n(q_4,q_3)} , \quad g_2 = g_1 , \quad g_3 = -\frac{1}{F_0(q_4,q_3)^2} - \sum_{n=1}^{\infty} \frac{4n}{F_n(q_4,q_3)^2} , \tag{B.66}$$

$$g_4 = \sum_{n=1}^{\infty} \frac{n(n+1)}{F_{n+1}(q_4,q_3)F_n(q_4,q_3)} , \quad g_5 = g_4 , \quad g_6 = -\sum_{n=1}^{\infty} \frac{2n^2}{F_n(q_4,q_3)^2} . \tag{B.67}$$

Plugging all into (B.65), we get

$$\begin{aligned} &\frac{1}{2|eB|} \lim_{W\to 0} \frac{d}{dW} \int \frac{d^2q_\perp}{(2\pi)^2} \operatorname{tr}[\tilde{G}_{p+q}\gamma_5 \tilde{G}_q \gamma_5] \\ &= \frac{1}{2\pi} \left(-\frac{1}{F_0(q_4,q_3)} + \frac{2}{F_1(q_4,q_3)} \right) + \frac{F_0(q_4,q_3)}{\pi} \sum_{n=1}^{\infty} \left(\frac{2n+1}{F_{n+1}(q_4,q_3)F_n(q_4,q_3)} - \frac{2n}{F_n(q_4,q_3)^2} \right) \\ &\quad + \frac{4|eB|}{\pi} \sum_{n=1}^{\infty} \left(\frac{n(n+1)}{F_{n+1}(q_4,q_3)F_n(q_4,q_3)} - \frac{n^2}{F_n(q_4,q_3)^2} \right) \end{aligned} \tag{B.68}$$

where we have deliberately grouped the series into parentheses so that the sums are convergent. We performed these sums over n with *Mathematica*, finding

$$\begin{aligned} &= \frac{1}{2\pi} \left(-\frac{1}{F_0(q_4,q_3)} + \frac{2}{F_1(q_4,q_3)} \right) + \frac{F_0(q_4,q_3)}{\pi} \frac{1}{4|eB|^2} \Big\{ 2D\psi^{(1)}(1+D) + \frac{1}{1+D} - 2 \Big\} \\ &\quad + \frac{4|eB|}{\pi} \frac{1}{4|eB|^2} \Big\{ D - D^2\psi^{(1)}(1+D) \Big\} \qquad \left(D \equiv \frac{F_0(q_4,q_3)}{2|eB|} \right) \end{aligned} \tag{B.69}$$

$$= -\frac{1}{2\pi F_0(q_4,q_3)} + \frac{1}{2\pi|eB|} , \tag{B.70}$$

where $\psi^{(1)}(x)$ is the first derivative of the digamma function.

Using $\tilde{\partial}_k F_0(q_4,q_3) = 2k\,\theta(k^2-q_3^2)$ one can easily show

$$\tilde{\partial}_k \left(\frac{1}{2|eB|} \lim_{W\to 0} \frac{d}{dW} \int \frac{d^2q_\perp}{(2\pi)^2} \operatorname{tr}[\tilde{G}_{p+q}\gamma_5 \tilde{G}_q \gamma_5] \right) = \frac{1}{\pi} \frac{k}{(q_4^2+k^2+2g^2\overline{\rho}_k)^2} \theta(k^2-q_3^2) . \tag{B.71}$$

Plugging this into (B.62) we finally obtain

$$\partial_k Z_k^\perp \Big|_{\text{fermi}} = -N_c g^2\, T \sum_{q_4:\,\text{odd}} \int \frac{dq_3}{2\pi} \left[\frac{1}{\pi} \frac{k}{(q_4^2+k^2+2g^2\overline{\rho}_k)^2} \theta(k^2-q_3^2) \right] \tag{B.72}$$

$$= -\frac{1}{\pi^2} N_c g^2 k^2\, T \sum_{q_4:\,\text{odd}} \frac{1}{(q_4^2+k^2+2g^2\overline{\rho}_k)^2} \tag{B.73}$$

$$= -\frac{1}{\pi^2} N_c g^2 k^2 \left(\frac{1}{4E_0(\overline{\rho}_k)^3} \tanh \frac{E_0(\overline{\rho}_k)}{2T} - \frac{1}{8E_0(\overline{\rho}_k)^2 T} \operatorname{sech}^2 \frac{E_0(\overline{\rho}_k)}{2T} \right) , \tag{B.74}$$

with $E_0(\overline{\rho}_k) = \sqrt{k^2 + 2g^2\overline{\rho}_k}$. The sum of (B.73) and (B.32) yields $\partial_k Z_k^\perp$ in (2.7).

B.2.2 Flow of $Z_k^\parallel$

Let us rewrite (B.47) as

$$\partial_k Z_k^\parallel\Big|_{\rm fermi} = -\frac{1}{2}N_c g^2\, T \sum_{q_4:\,\rm odd} \lim_{p\to 0}\frac{\partial^2}{\partial p_3^2}\int\frac{dq_3}{2\pi}\,\tilde\partial_k\int\frac{d^2q_\perp}{(2\pi)^2}\,{\rm tr}[\tilde G_{p+q}\gamma_5\tilde G_q\gamma_5]\,. \tag{B.75}$$

We shall carry out the calculations on the RHS in this order. Let us take the limit $p_1 \to 0$ (i.e., $W \to 0$) to focus on the p_3-dependence. Using (B.63) one can easily show that all terms in (B.60) with $|n-m| \geq 1$ vanish as $W \to 0$, leaving

$$\int\frac{d^2q_\perp}{(2\pi)^2}\,{\rm tr}[\tilde G_{p+q}\gamma_5\tilde G_q\gamma_5]\Big|_{W\to 0} = \sum_{n=0}^{\infty}\frac{1}{F_n(q_4,\mathbf{q}_3)F_n(q_4,q_3)}\left\{\alpha_n\frac{|eB|}{\pi}\mathbf{F}_0(q_4,q_3,\mathbf{q}_3) + \frac{4}{\pi}|eB|^2 n\right\}. \tag{B.76}$$

Then

$$\int\frac{dq_3}{2\pi}\,\tilde\partial_k\left(\int\frac{d^2q_\perp}{(2\pi)^2}\,{\rm tr}[\tilde G_{p+q}\gamma_5\tilde G_q\gamma_5]\Big|_{W\to 0}\right) = \mathfrak{X}_1 + \mathfrak{X}_2 + \mathfrak{X}_3\,, \tag{B.77}$$

with the definitions

$$\mathfrak{X}_1 \equiv -\int\frac{dq_3}{2\pi}\sum_{n=0}^{\infty}\frac{\tilde\partial_k F_n(q_4,\mathbf{q}_3)}{F_n(q_4,\mathbf{q}_3)^2F_n(q_4,q_3)}\left\{\alpha_n\frac{|eB|}{\pi}\mathbf{F}_0(q_4,q_3,\mathbf{q}_3) + \frac{4}{\pi}|eB|^2 n\right\}, \tag{B.78}$$

$$\mathfrak{X}_2 \equiv -\int\frac{dq_3}{2\pi}\sum_{n=0}^{\infty}\frac{\tilde\partial_k F_n(q_4,q_3)}{F_n(q_4,\mathbf{q}_3)F_n(q_4,q_3)^2}\left\{\alpha_n\frac{|eB|}{\pi}\mathbf{F}_0(q_4,q_3,\mathbf{q}_3) + \frac{4}{\pi}|eB|^2 n\right\}, \tag{B.79}$$

$$\mathfrak{X}_3 \equiv \int\frac{dq_3}{2\pi}\sum_{n=0}^{\infty}\frac{1}{F_n(q_4,\mathbf{q}_3)F_n(q_4,q_3)}\alpha_n\frac{|eB|}{\pi}\tilde\partial_k\mathbf{F}_0(q_4,q_3,\mathbf{q}_3)\,. \tag{B.80}$$

After elementary but quite lengthy calculations, we obtain (assuming $p_3 > 0$)

$$\begin{aligned}\mathfrak{X}_1 = &-\frac{1}{\pi^2}|eB|k(2k-p_3)\sum_{n=0}^{\infty}\frac{\alpha_n(q_4^2+k^2+2g^2\overline{\rho}_k)+4|eB|n}{[q_4^2+E_n(\overline{\rho}_k)^2]^3} + \frac{2}{\pi^2}|eB|k^3p_3\sum_{n=0}^{\infty}\frac{\alpha_n}{[q_4^2+E_n(\overline{\rho}_k)^2]^3}\\ &-\frac{2}{\pi}|eB|k\int_{-k-p_3}^{-k}\frac{dq_3}{2\pi}\sum_{n=0}^{\infty}\frac{\alpha_n(q_4^2-kq_3+2g^2\overline{\rho}_k)+4|eB|n}{[q_4^2+E_n(\overline{\rho}_k)^2]^2(q_4^2+q_3^2+2|eB|n+2g^2\overline{\rho}_k)}\,,\end{aligned} \tag{B.81}$$

$$\mathfrak{X}_2 = \mathfrak{X}_1\,, \tag{B.82}$$

$$\begin{aligned}\mathfrak{X}_3 = &-\frac{2}{\pi}|eB|\int_{-k-p_3}^{-k}\frac{dq_3}{2\pi}\sum_{n=0}^{\infty}\frac{\alpha_n q_3}{[q_4^2+E_n(\overline{\rho}_k)^2](q_4^2+q_3^2+2|eB|n+2g^2\overline{\rho}_k)}\\ &+\frac{1}{\pi^2}|eB|k(2k-3p_3)\sum_{n=0}^{\infty}\frac{\alpha_n}{[q_4^2+E_n(\overline{\rho}_k)^2]^2}\,,\end{aligned} \tag{B.83}$$

where we have used $E_n(\rho)$ defined in (2.10), and used

$$\tilde\partial_k F_n(q_4,q_3) = 2k\,\theta(k^2-q_3^2)\,, \tag{B.84}$$

$$\tilde\partial_k F_n(q_4,\mathbf{q}_3) = 2k\,\theta(k^2-\mathbf{q}_3^2)\,, \tag{B.85}$$

$$\tilde\partial_k\mathbf{F}_0(q_4,q_3,\mathbf{q}_3) = \mathbf{q}_3 q_3\left\{\frac{\theta(k^2-q_3^2)}{|q_3|}[1+r_k(\mathbf{q}_3)] + \frac{\theta(k^2-\mathbf{q}_3^2)}{|\mathbf{q}_3|}[1+r_k(q_3)]\right\}. \tag{B.86}$$

Note that the first line of (B.81) and the second line of (B.83) vanish in the limit $\lim_{p\to 0}\frac{\partial^2}{\partial p_3^2}$. Using this fact, we find

$$\lim_{p\to 0}\frac{\partial^2}{\partial p_3^2}(\mathfrak{X}_1+\mathfrak{X}_2+\mathfrak{X}_3)=\frac{1}{\pi^2}|eB|\sum_{n=0}^{\infty}\frac{\alpha_n}{[q_4^2+E_n(\overline{\rho}_k)^2]^2}\,. \tag{B.87}$$

Substituting this into (B.75) we finally arrive at

$$\partial_k Z_k^{\parallel}\Big|_{\text{fermi}}=-\frac{1}{2\pi^2}N_c g^2|eB|\,T\sum_{q_4:\,\text{odd}}\sum_{n=0}^{\infty}\frac{\alpha_n}{[q_4^2+E_n(\overline{\rho}_k)^2]^2}\,. \tag{B.88}$$

The sum of (B.88) and (B.34) yields $\partial_k Z_k^{\parallel}$ in (2.8).

To speed up numerical computation we analytically summed over n, with the result

$$\begin{aligned}\partial_k Z_k^{\parallel}\Big|_{\text{fermi}}=-\frac{N_c}{2\pi^2}g^2|eB|\Bigg\{&\frac{1}{4E_0(\overline{\rho}_k)^3}\tanh\frac{E_0(\overline{\rho}_k)}{2T}-\frac{1}{8E_0(\overline{\rho}_k)^2T}\mathrm{sech}^2\frac{E_0(\overline{\rho}_k)}{2T}\\&+\frac{T}{2|eB|^2}\sum_{q_4:\,\text{odd}}\psi^{(1)}\left(1+\frac{q_4^2+E_0(\overline{\rho}_k)^2}{2|eB|}\right)\Bigg\}.\end{aligned} \tag{B.89}$$

Since $\psi^{(1)}(x)\sim 1/x$ for $x\gg 1$, the sum is convergent.

C Flow of the Taylor coefficients of U_k

The flows (2.17) of parameters in the Taylor expansion of U_k depend on $\partial_k U_k'\big|_{\overline{\rho}_k}$ and $\partial_k U_k''\big|_{\overline{\rho}_k}$. The latter can be obtained from (2.6) by taking the derivative with ρ and substituting the polynomial expression (2.15). After elementary calculations, we arrive at

$$\begin{aligned}&\partial_k U_k'\Big|_{\overline{\rho}_k}\\&=-\frac{k^2}{8\pi^2}\left(1+\frac{k}{3}\frac{\partial_k Z_k^{\parallel}}{Z_k^{\parallel}}\right)\frac{a_k^{(2)}}{Z_k^{\perp}}\left\{\frac{\coth\left(\frac{1}{2T}\sqrt{k^2+\frac{a_k^{(1)}}{Z_k^{\parallel}}}\right)}{\sqrt{k^2+\frac{a_k^{(1)}}{Z_k^{\parallel}}}}+3\,\frac{\coth\left(\frac{1}{2T}\sqrt{k^2+\frac{a_k^{(1)}+2\overline{\rho}_k a_k^{(2)}}{Z_k^{\parallel}}}\right)}{\sqrt{k^2+\frac{a_k^{(1)}+2\overline{\rho}_k a_k^{(2)}}{Z_k^{\parallel}}}}\right\}\\&\quad-\frac{N_c}{2\pi^2}g^2k^2|eB|\sum_{n=0}^{\infty}\alpha_n\left(\frac{\mathrm{sech}^2\frac{E_n(\overline{\rho}_k)}{2T}}{2T\cdot E_n(\overline{\rho}_k)^2}-\frac{\tanh\frac{E_n(\overline{\rho}_k)}{2T}}{E_n(\overline{\rho}_k)^3}\right),\end{aligned} \tag{C.1}$$

and

$$
\begin{aligned}
&\partial_k U_k''\Big|_{\bar\rho_k} \\
&= \frac{k^2}{8\pi^2}\left(1+\frac{k}{3}\frac{\partial_k Z_k^{\parallel}}{Z_k^{\parallel}}\right)\frac{\left(a_k^{(2)}\right)^2}{2Z_k^{\perp}Z_k^{\parallel}}\left\{\frac{\coth\left(\frac{1}{2T}\sqrt{k^2+\frac{a_k^{(1)}}{Z_k^{\parallel}}}\right)}{\left(k^2+\frac{a_k^{(1)}}{Z_k^{\parallel}}\right)^{3/2}}+\frac{\operatorname{csch}^2\left(\frac{1}{2T}\sqrt{k^2+\frac{a_k^{(1)}}{Z_k^{\parallel}}}\right)}{2T\left(k^2+\frac{a_k^{(1)}}{Z_k^{\parallel}}\right)}\right. \\
&\qquad\left.+\frac{9\coth\left(\frac{1}{2T}\sqrt{k^2+\frac{a_k^{(1)}+2\bar\rho_k a_k^{(2)}}{Z_k^{\parallel}}}\right)}{\left(k^2+\frac{a_k^{(1)}+2\bar\rho_k a_k^{(2)}}{Z_k^{\parallel}}\right)^{3/2}}+\frac{9\operatorname{csch}^2\left(\frac{1}{2T}\sqrt{k^2+\frac{a_k^{(1)}+2\bar\rho_k a_k^{(2)}}{Z_k^{\parallel}}}\right)}{2T\left(k^2+\frac{a_k^{(1)}+2\bar\rho_k a_k^{(2)}}{Z_k^{\parallel}}\right)}\right\} \\
&\quad-\frac{N_c}{2\pi^2}g^4k^2|eB|\sum_{n=0}^{\infty}\alpha_n\left(-\frac{3}{2T}\frac{\operatorname{sech}^2\frac{E_n(\bar\rho_k)}{2T}}{E_n(\bar\rho_k)^4}+3\frac{\tanh\frac{E_n(\bar\rho_k)}{2T}}{E_n(\bar\rho_k)^5}-\frac{1}{2T^2}\frac{\operatorname{sech}^2\frac{E_n(\bar\rho_k)}{2T}\tanh\frac{E_n(\bar\rho_k)}{2T}}{E_n(\bar\rho_k)^3}\right).
\end{aligned}
\tag{C.2}
$$

The convergence of the Landau level sums in (C.1) and (C.2) is rather slow, due to the terms $\frac{\tanh\frac{E_n(\bar\rho_k)}{2T}}{E_n(\bar\rho_k)^3}$ and $\frac{\tanh\frac{E_n(\bar\rho_k)}{2T}}{E_n(\bar\rho_k)^5}$ that decay only slowly especially when $k^2+2g^2\bar\rho_k \gg 2|eB|$. From a computational point of view, it is advantageous to split the zero temperature part from the thermal part as $\tanh\frac{E_n(\bar\rho_k)}{2T} = 1+\left(\tanh\frac{E_n(\bar\rho_k)}{2T}-1\right)$ and perform the summation in the zero temperature part analytically as

$$
\sum_{n=0}^{\infty}\frac{\alpha_n}{E_n(\bar\rho_k)^3} = -\frac{1}{E_0(\bar\rho_k)^3}+\frac{1}{\sqrt{2}|eB|^{3/2}}\zeta\left(\frac{3}{2},\frac{E_0(\bar\rho_k)^2}{2|eB|}\right), \tag{C.3}
$$

$$
\sum_{n=0}^{\infty}\frac{\alpha_n}{E_n(\bar\rho_k)^5} = -\frac{1}{E_0(\bar\rho_k)^5}+\frac{1}{2\sqrt{2}|eB|^{5/2}}\zeta\left(\frac{5}{2},\frac{E_0(\bar\rho_k)^2}{2|eB|}\right), \tag{C.4}
$$

where $\zeta(x,y)$ is the Hurwitz zeta function. Then all the terms in the remainder are suppressed by a Boltzmann factor $\sim \mathrm{e}^{-E_n(\bar\rho_k)/T}$ and only a small number of Landau levels contribute to the sum. We found that this trick speeds up numerical computation of the flow equation considerably.

References

[1] K. Fukushima and T. Hatsuda, *The phase diagram of dense QCD*, *Rept. Prog. Phys.* **74** (2011) 014001, [arXiv:1005.4814].

[2] R. C. Duncan and C. Thompson, *Formation of very strongly magnetized neutron stars - implications for gamma-ray bursts*, *Astrophys.J.* **392** (1992) L9.

[3] D. Grasso and H. R. Rubinstein, *Magnetic fields in the early universe*, *Phys.Rept.* **348** (2001) 163–266, [astro-ph/0009061].

[4] V. Skokov, A. Y. Illarionov, and V. Toneev, *Estimate of the magnetic field strength in heavy-ion collisions*, *Int.J.Mod.Phys.* **A24** (2009) 5925–5932, [arXiv:0907.1396].

[5] H. Suganuma and T. Tatsumi, *ON THE BEHAVIOR OF SYMMETRY AND PHASE TRANSITIONS IN A STRONG ELECTROMAGNETIC FIELD*, *Annals Phys.* **208** (1991) 470–508.

[6] K. Klimenko, *Three-dimensional Gross-Neveu model in an external magnetic field*, *Theor.Math.Phys.* **89** (1992) 1161–1168.

[7] K. Klimenko, *Three-dimensional Gross-Neveu model at nonzero temperature and in an external magnetic field*, *Z.Phys.* **C54** (1992) 323–330.

[8] V. Gusynin, V. Miransky, and I. Shovkovy, *Catalysis of dynamical flavor symmetry breaking by a magnetic field in (2+1)-dimensions*, *Phys.Rev.Lett.* **73** (1994) 3499–3502, [hep-ph/9405262].

[9] V. Gusynin, V. Miransky, and I. Shovkovy, *Dynamical flavor symmetry breaking by a magnetic field in (2+1)-dimensions*, *Phys.Rev.* **D52** (1995) 4718–4735, [hep-th/9407168].

[10] V. Gusynin, V. Miransky, and I. Shovkovy, *Dimensional reduction and dynamical chiral symmetry breaking by a magnetic field in (3+1)-dimensions*, *Phys.Lett.* **B349** (1995) 477–483, [hep-ph/9412257].

[11] V. Gusynin, V. Miransky, and I. Shovkovy, *Dimensional reduction and catalysis of dynamical symmetry breaking by a magnetic field*, *Nucl.Phys.* **B462** (1996) 249–290, [hep-ph/9509320].

[12] D. Ebert and K. Klimenko, *Quark droplets stability induced by external magnetic field*, *Nucl.Phys.* **A728** (2003) 203–225, [hep-ph/0305149].

[13] T. Inagaki, D. Kimura, and T. Murata, *Four fermion interaction model in a constant magnetic field at finite temperature and chemical potential*, *Prog.Theor.Phys.* **111** (2004) 371–386, [hep-ph/0312005].

[14] E. S. Fraga and A. J. Mizher, *Chiral transition in a strong magnetic background*, *Phys.Rev.* **D78** (2008) 025016, [arXiv:0804.1452].

[15] D. Menezes, M. Benghi Pinto, S. Avancini, A. Perez Martinez, and C. Providencia, *Quark matter under strong magnetic fields in the Nambu-Jona-Lasinio Model*, *Phys.Rev.* **C79** (2009) 035807, [arXiv:0811.3361].

[16] D. Menezes, M. Benghi Pinto, S. Avancini, and C. Providencia, *Quark matter under strong magnetic fields in the su(3) Nambu-Jona-Lasinio Model*, *Phys.Rev.* **C80** (2009) 065805, [arXiv:0907.2607].

[17] J. K. Boomsma and D. Boer, *The Influence of strong magnetic fields and instantons on the phase structure of the two-flavor NJL model*, *Phys.Rev.* **D81** (2010) 074005, [arXiv:0911.2164].

[18] K. Fukushima, M. Ruggieri, and R. Gatto, *Chiral magnetic effect in the PNJL model*, *Phys.Rev.* **D81** (2010) 114031, [arXiv:1003.0047].

[19] A. J. Mizher, M. Chernodub, and E. S. Fraga, *Phase diagram of hot QCD in an external magnetic field: possible splitting of deconfinement and chiral transitions*, *Phys.Rev.* **D82** (2010) 105016, [arXiv:1004.2712].

[20] S. Fayazbakhsh and N. Sadooghi, *Phase diagram of hot magnetized two-flavor color superconducting quark matter*, *Phys.Rev.* **D83** (2011) 025026, [arXiv:1009.6125].

[21] R. Gatto and M. Ruggieri, *Deconfinement and Chiral Symmetry Restoration in a Strong Magnetic Background*, *Phys.Rev.* **D83** (2011) 034016, [arXiv:1012.1291].

[22] B. Chatterjee, H. Mishra, and A. Mishra, *Vacuum structure and chiral symmetry breaking in strong magnetic fields for hot and dense quark matter*, *Phys.Rev.* **D84** (2011) 014016, [arXiv:1101.0498].

[23] M. Frasca and M. Ruggieri, *Magnetic Susceptibility of the Quark Condensate and Polarization from Chiral Models*, *Phys.Rev.* **D83** (2011) 094024, [arXiv:1103.1194].

[24] A. Rabhi and C. Providencia, *Quark matter under strong magnetic field in chiral models*, *Phys.Rev.* **C83** (2011) 055801, [arXiv:1104.1512].

[25] K. Kashiwa, *Entanglement between chiral and deconfinement transitions under strong uniform magnetic background field*, *Phys.Rev.* **D83** (2011) 117901, [arXiv:1104.5167].

[26] J. O. Andersen and R. Khan, *Chiral transition in a magnetic field and at finite baryon density*, *Phys.Rev.* **D85** (2012) 065026, [arXiv:1105.1290].

[27] V. Skokov, *Phase diagram in an external magnetic field beyond a mean-field approximation*, *Phys.Rev.* **D85** (2012) 034026, [arXiv:1112.5137].

[28] D. D. Scherer and H. Gies, *Renormalization Group Study of Magnetic Catalysis in the 3d Gross-Neveu Model*, *Phys.Rev.* **B85** (2012) 195417, [arXiv:1201.3746].

[29] K. Fukushima and J. M. Pawlowski, *Magnetic catalysis in hot and dense quark matter and quantum fluctuations*, *Phys.Rev.* **D86** (2012) 076013, [arXiv:1203.4330].

[30] J. O. Andersen and A. Tranberg, *The Chiral transition in a magnetic background: Finite density effects and the functional renormalization group*, *JHEP* **1208** (2012) 002, [arXiv:1204.3360].

[31] S. Fayazbakhsh, S. Sadeghian, and N. Sadooghi, *Properties of neutral mesons in a hot and magnetized quark matter*, *Phys.Rev.* **D86** (2012) 085042, [arXiv:1206.6051].

[32] S. Fayazbakhsh and N. Sadooghi, *Weak decay constant of neutral pions in a hot and magnetized quark matter*, *Phys.Rev.* **D88** (2013) 065030, [arXiv:1306.2098].

[33] G. N. Ferrari, A. F. Garcia, and M. B. Pinto, *Chiral Transition Within Effective Quark Models Under Magnetic Fields*, *Phys.Rev.* **D86** (2012) 096005, [arXiv:1207.3714].

[34] F. Preis, A. Rebhan, and A. Schmitt, *Inverse magnetic catalysis in field theory and gauge-gravity duality*, *Lect.Notes Phys.* **871** (2013) 51–86, [arXiv:1208.0536].

[35] J. O. Andersen, W. R. Naylor, and A. Tranberg, *Chiral and deconfinement transitions in a magnetic background using the functional renormalization group with the Polyakov loop*, arXiv:1311.2093.

[36] E. J. Ferrer, V. de la Incera, I. Portillo, and M. Quiroz, *A new look at the QCD ground state in a magnetic field*, arXiv:1311.3400.

[37] R. Gatto and M. Ruggieri, *Quark Matter in a Strong Magnetic Background*, *Lect.Notes Phys.* **871** (2013) 87–119, [arXiv:1207.3190].

[38] I. A. Shovkovy, *Magnetic Catalysis: A Review*, *Lect.Notes Phys.* **871** (2013) 13–49, [arXiv:1207.5081].

[39] P. Buividovich, M. Chernodub, E. Luschevskaya, and M. Polikarpov, *Numerical study of chiral symmetry breaking in non-Abelian gauge theory with background magnetic field*, *Phys.Lett.* **B682** (2010) 484–489, [arXiv:0812.1740].

[40] M. D'Elia, S. Mukherjee, and F. Sanfilippo, *QCD Phase Transition in a Strong Magnetic Background*, *Phys.Rev.* **D82** (2010) 051501, [arXiv:1005.5365].

[41] M. D'Elia and F. Negro, *Chiral Properties of Strong Interactions in a Magnetic Background*, *Phys.Rev.* **D83** (2011) 114028, [arXiv:1103.2080].

[42] V. Braguta, P. Buividovich, M. Chernodub, A. Y. Kotov, and M. Polikarpov, *Electromagnetic superconductivity of vacuum induced by strong magnetic field: numerical evidence in lattice gauge theory*, *Phys.Lett.* **B718** (2012) 667–671, [arXiv:1104.3767].

[43] G. Bali, F. Bruckmann, G. Endrodi, Z. Fodor, S. Katz, et al., *The QCD phase diagram for external magnetic fields*, *JHEP* **1202** (2012) 044, [arXiv:1111.4956].

[44] E.-M. Ilgenfritz, M. Kalinowski, M. Muller-Preussker, B. Petersson, and A. Schreiber, *Two-color QCD with staggered fermions at finite temperature under the influence of a magnetic field*, *Phys.Rev.* **D85** (2012) 114504, [arXiv:1203.3360].

[45] E. Luschevskaya and O. Larina, *The ρ and a mesons in a strong abelian magnetic field in SU(2) lattice gauge theory*, arXiv:1203.5699.

[46] G. Bali, F. Bruckmann, G. Endrodi, Z. Fodor, S. Katz, et al., *QCD quark condensate in external magnetic fields*, *Phys.Rev.* **D86** (2012) 071502, [arXiv:1206.4205].

[47] G. Bali, F. Bruckmann, M. Constantinou, M. Costa, G. Endrodi, et al., *Magnetic susceptibility of QCD at zero and at finite temperature from the lattice*, *Phys.Rev.* **D86** (2012) 094512, [arXiv:1209.6015].

[48] G. Bali, F. Bruckmann, G. Endrodi, F. Gruber, and A. Schaefer, *Magnetic field-induced gluonic (inverse) catalysis and pressure (an)isotropy in QCD*, *JHEP* **1304** (2013) 130, [arXiv:1303.1328].

[49] C. Bonati, M. D'Elia, M. Mariti, F. Negro, and F. Sanfilippo, *Magnetic Susceptibility of Strongly Interacting Matter across the Deconfinement Transition*, *Phys.Rev.Lett.* **111** (2013) 182001, [arXiv:1307.8063].

[50] L. Levkova and C. DeTar, *Quark-gluon plasma in an external magnetic field*, *Phys.Rev.Lett.* **112** (2014) 012002, [arXiv:1309.1142].

[51] E. M. Ilgenfritz, M. Muller-Preussker, B. Petersson, and A. Schreiber, *Magnetic catalysis (and inverse catalysis) at finite temperature in two-color lattice QCD*, arXiv:1310.7876.

[52] C. Bonati, M. D'Elia, M. Mariti, F. Negro, and F. Sanfilippo, *Magnetic susceptibility and equation of state of $N_f = 2 + 1$ QCD with physical quark masses*, arXiv:1310.8656.

[53] M. D'Elia, *Lattice QCD Simulations in External Background Fields*, *Lect.Notes Phys.* **871** (2013) 181–208, [arXiv:1209.0374].

[54] V. Bornyakov, P. Buividovich, N. Cundy, O. Kochetkov, and A. Schäfer, *Deconfinement transition in two-flavour lattice QCD with dynamical overlap fermions in an external magnetic field*, arXiv:1312.5628.

[55] K. Fukushima and Y. Hidaka, *Magnetic Catalysis vs Magnetic Inhibition*, *Phys.Rev.Lett.* **110** (2013) 031601, [arXiv:1209.1319].

[56] T. Kojo and N. Su, *The quark mass gap in a magnetic field*, *Phys.Lett.* **B720** (2013) 192–197, [arXiv:1211.7318].

[57] F. Bruckmann, G. Endrodi, and T. G. Kovacs, *Inverse magnetic catalysis and the Polyakov loop*, *JHEP* **1304** (2013) 112, [arXiv:1303.3972].

[58] J. Chao, P. Chu, and M. Huang, *Inverse magnetic catalysis induced by sphalerons*, *Phys.Rev.* **D88** (2013) 054009, [arXiv:1305.1100].

[59] C. Wetterich, *Exact evolution equation for the effective potential*, *Phys.Lett.* **B301** (1993) 90–94.

[60] J. Berges, N. Tetradis, and C. Wetterich, *Nonperturbative renormalization flow in quantum field theory and statistical physics*, *Phys.Rept.* **363** (2002) 223–386, [hep-ph/0005122].

[61] J. M. Pawlowski, *Aspects of the functional renormalisation group*, *Annals Phys.* **322** (2007) 2831–2915, [hep-th/0512261].

[62] B. Delamotte, *An Introduction to the nonperturbative renormalization group*, *Lect.Notes Phys.* **852** (2012) 49–132, [cond-mat/0702365].

[63] J. Braun, *Fermion Interactions and Universal Behavior in Strongly Interacting Theories*, *J.Phys.* **G39** (2012) 033001, [arXiv:1108.4449].

[64] R. D. Pisarski and M. Tytgat, *Propagation of cool pions*, *Phys.Rev.* **D54** (1996) 2989–2993, [hep-ph/9604404].

[65] D. Son and M. A. Stephanov, *Pion propagation near the QCD chiral phase transition*, *Phys.Rev.Lett.* **88** (2002) 202302, [hep-ph/0111100].

[66] D. Son and M. A. Stephanov, *Real time pion propagation in finite temperature QCD*, *Phys.Rev.* **D66** (2002) 076011, [hep-ph/0204226].

[67] D. Jungnickel and C. Wetterich, *Effective action for the chiral quark-meson model*, *Phys.Rev.* **D53** (1996) 5142–5175, [hep-ph/9505267].

[68] J. Berges, D. Jungnickel, and C. Wetterich, *Two flavor chiral phase transition from nonperturbative flow equations*, *Phys.Rev.* **D59** (1999) 034010, [hep-ph/9705474].

[69] T. R. Morris, *Equivalence of local potential approximations*, *JHEP* **0507** (2005) 027, [hep-th/0503161].

[70] T. R. Morris and J. F. Tighe, *Convergence of derivative expansions of the renormalization group*, *JHEP* **9908** (1999) 007, [hep-th/9906166].

[71] J. Braun, *Thermodynamics of QCD low-energy models and the derivative expansion of the effective action*, *Phys.Rev.* **D81** (2010) 016008, [arXiv:0908.1543].

[72] B.-J. Schaefer and J. Wambach, *The Phase diagram of the quark meson model*, *Nucl.Phys.* **A757** (2005) 479–492, [nucl-th/0403039].

[73] V. Skokov, B. Stokic, B. Friman, and K. Redlich, *Meson fluctuations and thermodynamics of the Polyakov loop extended quark-meson model*, *Phys.Rev.* **C82** (2010) 015206, [arXiv:1004.2665].

[74] T. K. Herbst, J. M. Pawlowski, and B.-J. Schaefer, *The phase structure of the Polyakov–quark-meson model beyond mean field*, *Phys.Lett.* **B696** (2011) 58–67, [arXiv:1008.0081].

[75] B. Stokic, B. Friman, and K. Redlich, *The Functional Renormalization Group and O(4) scaling*, *Eur.Phys.J.* **C67** (2010) 425–438, [arXiv:0904.0466].

[76] Y. Hidaka and A. Yamamoto, *Charged vector mesons in a strong magnetic field*, *Phys.Rev.* **D87** (2013) 094502, [arXiv:1209.0007].

[77] I. Shushpanov and A. V. Smilga, *Quark condensate in a magnetic field*, *Phys.Lett.* **B402** (1997) 351–358, [hep-ph/9703201].

[78] N. O. Agasian and I. Shushpanov, *Gell-Mann-Oakes-Renner relation in a magnetic field at finite temperature*, *JHEP* **0110** (2001) 006, [hep-ph/0107128].

[79] J. O. Andersen, *Thermal pions in a magnetic background*, *Phys.Rev.* **D86** (2012) 025020, [arXiv:1202.2051].

[80] J. O. Andersen, *Chiral perturbation theory in a magnetic background - finite-temperature effects*, *JHEP* **1210** (2012) 005, [arXiv:1205.6978].

[81] V. Orlovsky and Y. Simonov, *Nambu-Goldstone mesons in strong magnetic field*, *JHEP* **1309** (2013) 136, [arXiv:1306.2232].

[82] J. O. Andersen and A. A. Cruz, *Two-color QCD in a strong magnetic field: The role of the Polyakov loop*, *Phys.Rev.* **D88** (2013) 025016, [arXiv:1211.7293].

[83] J. S. Schwinger, *On gauge invariance and vacuum polarization*, *Phys.Rev.* **82** (1951) 664–679.